UNDERSTANDING INTERPLANETARY CORONAL MASS EJECTION SIGNATURES

Report of Working Group B

R. F. WIMMER-SCHWEINGRUBER[1,*], N. U. CROOKER[2], A. BALOGH[3], V. BOTHMER[4], R. J. FORSYTH[3], P. GAZIS[5], J. T. GOSLING[6], T. HORBURY[3], A. KILCHENMANN[7], I. G. RICHARDSON[8], J. D. RICHARDSON[9], P. RILEY[10], L. RODRIGUEZ[4], R. VON STEIGER[7], P. WURZ[11], and T. H. ZURBUCHEN[12]

[1]*Institut für Experimentelle und Angewandte Physik, Extraterrestrische Physik, Christian-Albrechts-Universityät zu Kiel, Germany*

[2]*Center for Space Physics, Boston University, Boston, MA, USA*

[3]*The Blackett Laboratory, Imperial College London, United Kingdom*

[4]*Max-Planck-Institut für Sonnensystemforschung, Lindau, Germany*

[5]*San Jose State University Foundation, NASA Ames Research Center, Moffett Field, CA, USA*

[6]*Laboratory for Atmospheric and Space Physicsm University of Colorado, Boulder, CO, USA*

[7]*International Space Science Institute, Bern, Switzerland*

[8]*NASA Goddard Space Flight Center, Greenbelt, MD, USA*

[9]*Massachusets Institute of Technology, Cambridge, MA, USA*

[10]*Science Applications International Corporation, San Diego, CA, USA*

[11]*Physikalisches Institut, Universität Bern, Switzerland*

[12]*Dept. of Atmosph. ,Oceanic, and Space Sciences, University of Michigan, Ann Arbor, MI, USA*

([*]Author for correspondence: E-mail: wimmer@physik.uni-kiel.de)

(Received 30 November 2005; Accepted in final form 24 May 2006)

Abstract. While interplanetary coronal mass ejections (ICMEs) are understood to be the heliospheric counterparts of CMEs, with signatures undeniably linked to the CME process, the variability of these signatures and questions about mapping to observed CME features raise issues that remain on the cutting edge of ICME research. These issues are discussed in the context of traditional understanding, and recent results using innovative analysis techniques are reviewed.

Keywords: coronal mass ejections, interplanetary physics, solar wind

1. Introduction

Coronal mass ejections (CMEs) and their interplanetary manifestations, interplanetary coronal mass injections (ICMEs,) are still poorly understood entities. A decade ago, Schwenn (1996) gave an extensive list of unsolved problems and questions. Since then, the Solar and Heliospheric Observatory (SOHO) has much improved and to some extent revolutionized our understanding of CMEs and ICMEs. Our current knowledge of the relation of solar observables with ICMEs is discussed by Crooker and Horbury (2006) and Forsyth *et al.* (2006) in this volume. This paper focuses on recent progress in understanding in-situ signatures of ICMEs, building upon the introductory paper by Zurbuchen and Richardson (2006, this volume).

Space Science Reviews (2006) 123: 177–216
DOI: 10.1007/s11214-006-9017-x

ICME identification is not always straightforward, as will become apparent in this paper. Progress toward the unambiguous in-situ identification of ICMEs is of considerable scientific interest and is important to space weather applications (see Siscoe, 2006, this volume).

Ideally, the observation of CMEs and the developing ICMEs would take place in the innermost heliosphere, at a distance of a few solar radii using a fleet of several spacecraft. There, interactions with the ambient solar wind would not have had much chance of modifying the original plasma state of the CME, thus allowing a more direct linkage of remotely sensed structures with in-situ observations. In the real world, we have a plethora of observations, both in situ and remote, the latter mainly from the vicinity of the Earth, at 1 AU, with some observations at other heliocentric distances (e. g., Helios, Ulysses, Voyager, or Pioneer). This paper begins by discussing progress in understanding these various in situ signatures, mainly at 1 AU and briefly summarizes the ICME detection algorithm used on the Genesis spacecraft as an application. Section 3 discusses the detection of boundaries and multiple ICMEs, while Section 4 discusses inferences about the ICME's three-dimensional structure. Finally, Section 5 discusses other solar wind transients – not every unusual solar wind parcel is necessarily an ICME.

2. Signatures of ICMEs with In-Situ Data

This section addresses how different signatures can be used to identify ICMEs in situ and also mentions pitfalls that may arise when blindly applying these signatures. An ICME brings several structures past a spacecraft, all with their own signatures. Figure 2 of Zurbuchen and Richardson (2006, this volume) shows an idealized sketch of an ICME. Fast ICMEs will tend to drive a shock, which is not a signature of the ICME proper, but, nevertheless, a convenient, often-used and reasonably well-understood signature associated with many ICMEs. This shock can accelerate particles. The turbulence in the sheath following the shock modulates their propagation and is an important ingredient in the acceleration process. The boundary between the trailing edge of the sheath and the ICME can sometimes be difficult to identify. This may be due partly to the dynamic nature of ICME propagation, and possibly to evolution with time, e. g., by reconnection (e. g., Cargill and Schmidt, 2002; Gosling *et al.*, 2005). Moreover, different in-situ signatures do not necessarily give the same boundaries. The internal structure of ICMEs may be highly inhomogeneous, again resulting in difficulties identifying substructures and boundaries with different signatures.

2.1. Charge-State Composition

Solar wind in situ ionic observations provide a remote measure of the thermodynamic state of the solar wind source region. They therefore provide a unique,

useful way to relate in-situ plasma and field observations to their respective source (e.g., Hundhausen, 1968; Geiss *et al.*, 1995). Early observations of heavy ions in the solar wind, such as singly ionized helium or oxygen charge states (e.g., Bame *et al.*, 1968), provided a glimpse of the richness of ionic compositional data (see also Zurbuchen and Richardson (2006), this volume, for more references).

The relationship between enhanced ion charge states and ICMEs was first established when high ionization states of oxygen and iron were detected following interplanetary shocks (Bame *et al.*, 1979; Fenimore, 1980; Ipavich *et al.*, 1986). Bame *et al.* (1979) attributed these enhanced charge states to flare-heated coronal gas, an explanation recently explored by Lepri and Zurbuchen (2004). The magnetic bottle ICME (see Alexander *et al.*, 2006, this volume) was used to explain these and other post-shock phenomena (see Figure 2 of Zurbuchen and Richardson, 2006, this volume). Fenimore (1980) showed that other types of solar wind flows were related to their ionization states, with the hottest periods being those showing ICME signatures. Nevertheless, only a few ICME-related periods showed high freezing-in temperatures. These temperatures are determined by a competition between ionization/recombination times and the expansion time for the solar wind (Hundhausen *et al.*, 1968). They are derived from ionic charge-state pairs (e.g., O^{7+}/O^{6+}) and usually based on the assumption of equilibrium ionization and recombination in a Maxwellian electron gas. The study of Fenimore (1980) was limited by the use of electrostatic analyzers. More recent, dedicated instruments (e.g., the Solar Wind Ion Composition Spectrometers (SWICS) on ACE (Advanced Composition Explorer) and Ulysses) can measure the solar wind ionic composition under all circumstances. Results from these instruments have revealed that, indeed, the majority of all ICMEs are associated with elevated ionic charge states (e.g., Galvin *et al.*, 1997; Wimmer-Schweingruber *et al.*, 1999; Henke *et al.*, 2001; Lepri *et al.*, 2001; Zurbuchen *et al.*, 2003, Richardson and Cane, 2004; Rodriguez *et al.*, 2004; Zurbuchen *et al.*, 2003; Lepri and Zurbuchen, 2004). Henke *et al.* (2001), Rodriguez *et al.* (2004), and Richardson and Cane (2004) showed that high oxygen charge states are preferentially associated with the subset of ICMEs showing a magnetic cloud (MC) structure (see Figure 2). The observed elevated charge states suggest a direct linkage between ICME plasma and flares accompanying the related CMEs at the Sun. Such associations were found in ICME-CME analyses by Lepri and Zurbuchen (2004) and Reinard (2005). On the other hand, ICMEs at high latitudes do not necessarily exhibit elevated charge states (Neukomm, 1998).

Although extremely rare, ICMEs with unusually low charge states have also been reported. These were mostly identified based on the occurrence of singly charged He. The events described by Schwenn *et al.* (1980) and Gosling *et al.* (1980) had a He^{+}/He^{2+} ratio of up to 0.3, that is, nearly two orders of magnitude larger than that found originally by Bame *et al.* (1968). The explanation provided for such low charge states, which imply low coronal temperatures, was the presence of prominence material of chromospheric origin. These and other periods of abnormally low charge states were also analyzed by Zwickl *et al.* (1982).

These authors found periods in which both high and low ionization states were present, indicating mixing of the plasma and spatial inhomogeneity within these events and raising questions about the prominence interpretation. The existence of mixed (hot and cold) charge states during a He^+ rich event was also described by Gloeckler *et al.* (1999) and Skoug *et al.* (1999). The heavy ion charge-state composition showed clear evidence of unusually elevated charge states, typical of those found in ICMEs, throughout the most extended and most intense interval of enhanced He^+/He^{2+} ratio ever measured. The interpretation of these mixed charge states is still pending. More recently, Zurbuchen *et al.* (2005) analyzed the January 9, 2005, ICME associated with a CME accompanied by a prominence eruption on January 5th. The relation between the ICME and eruptive filament is suggested by its unique ionic composition, indicating coronal source temperatures well below 10^5 K. The time period with unusually cold ionic composition exhibited unusual elemental composition, with enhancements of O relative to He and Fe and was associated with a flux-rope-like magnetic field. Observations of this type may prove to be critical in distinguishing between CME initiation models.

2.2. Elemental Abundances

The classic ICME composition signature is an enhanced He/H abundance ratio (He/H $\geq$ 6%–8%), which may reach ~25% or more (Hirshberg *et al.*, 1970, 1972; Neugebauer, 1981; Borrini *et al.*, 1982). The He/H ratio in the normal solar wind ranges between 3% and about 5% (e.g., Neugebauer, 1981; Schwenn, 1990) and should be compared with the photospheric or solar value of around 10%. Obviously, some process is fractionating the solar wind He content and appears to act in the chromosphere and/or low corona (Laming and Feldman, 2001). One mechanism that has been proposed is inefficient Coulomb drag (Geiss *et al.*, 1970) in which helium experiences a smaller proton drag force than other heavy ions and is fractionated against the bulk solar wind protons. This in turn must lead to an enrichment of helium in the chromosphere and/or low corona since it is already ionized at this height and cannot be lost to the photosphere, where it would be incorporated into the near-infinite mass of the outer convective zone. The helium enhancement in ICMEs has been attributed to a "cleaning out" of helium left behind in the low corona by the solar wind. However, it is far from clear exactly how and where such a helium accumulation is produced and how it can persist for any length of time until it is ejected with a CME. Figure 2, discussed below, shows that about 30% of all ICMEs show this enhancement of He/H above 6% and that this fraction appears to be somewhat higher in magnetic clouds. Other compositional anomalies have also been reported (Bame *et al.*, 1979; Mitchell *et al.*, 1983; Ipavich *et al.*, 1986; Zurbuchen and Richardson, 2006).

Nevertheless, as can be seen in Figure 1, discussed below, many ICMEs, especially high-latitude ICMEs, do not show an elemental composition different from

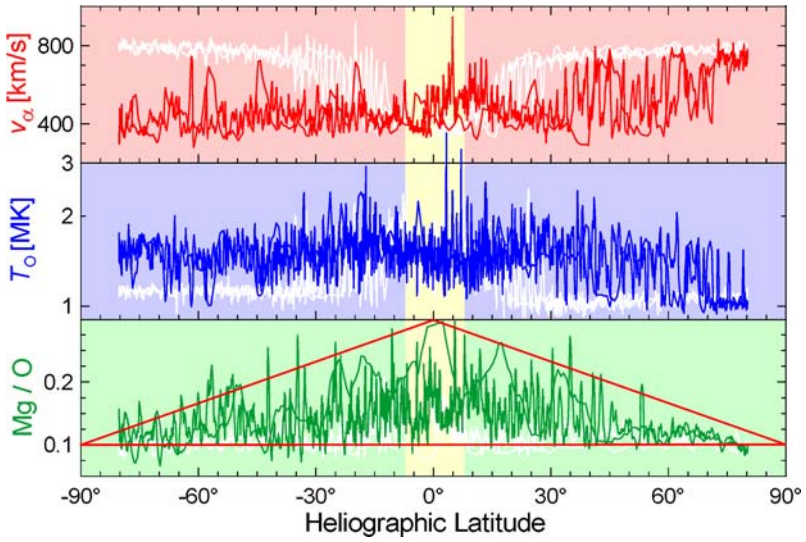

Figure 1. Ulysses-SWICS solar wind parameters from the second, solar maximum, polar orbit: alpha-particle speed (top), oxygen freeze-in temperature, T_O, (middle), and Mg/O abundance ratio (bottom). The distribution of fast and slow solar wind, which was well ordered by latitude for the first, solar minimum, pass (values shaded in white), looks drastically changed. The three "outliers" in T_O on the rightmost edge of the diagram correspond to three ICMEs detected by Ulysses at high latitudes. Remarkably, their unusually hot ionic composition is not reflected by the FIP enhancement in Mg/O that would be expected even in the normal slow solar wind.

the surrounding solar wind. Therefore, it seems fair to assume that the same basic first ionisation potential (FIP) fractionation mechanism applies to CME material as to the quasi-stationary solar wind (von Steiger, 1998). This process appears to separate neutral atoms from charged ions in the chromosphere and/or lower corona (Geiss, 1982). However, some ICMEs, at least some observed in the ecliptic plane, do show a much stronger fractionation (e.g., Wurz *et al.*, 1998; Gloeckler *et al.*, 1999; Wurz *et al.*, 2001), so there must be additional fractionation acting on the ejected material in addition to the normal solar wind fractionation. This may be either the same mechanism (the FIP effect) but operating more strongly or for a longer time (Widing and Feldman, 2001), or an additional, different mechanism that is operating on the pre-CME material. In some cases, especially for magnetic clouds, ICMEs show a mass-fractionated composition with an enhancement of heavy elements that cannot be understood in terms of FIP fractionation models (Wurz *et al.*, 2001). Wurz *et al.* (2000) have presented a model of how this mass fractionation might be explained. Nevertheless, such mass-fractionated ICMEs are rare events although they appear to be more frequent in magnetic clouds (Wurz *et al.*, 2001).

An interesting point in this context is illustrated in Figure 1, which shows three solar wind parameters obtained with the SWICS instrument on Ulysses as a function

of heliographic latitude. From top to bottom:these are bulk He^{2+} speed, v_α, oxygen freeze-in temperature, T_O, and the Mg/O elemental abundance ratio, which may be taken as a proxy for the FIP fractionation factor (the Fe/O ratio serves the same purpose and looks qualitatively similar). The white curves in the background show the values measured during Ulysses' first polar pass at solar minimum. Close inspection shows two data points for each latitude, one for the slow and one for the fast pass. The white curves contrast with the colored curves, which show the same quantities but measured during the second polar orbit of Ulysses at solar maximum. Slow, variable solar wind dominates during most of that orbit except for a portion at high northern latitudes (rightmost part of the panel), where the newly forming polar coronal hole of cycle 23 is revealed by its elevated solar wind speed and low freeze-in temperature. One also sees 3 embedded ICMEs – the three rightmost spikes visible in freeze-in temperature (but not in Mg/O). Not surprisingly, the Mg/O ratio is low in that part of the second orbit, as it was in the polar coronal holes during the first, solar minimum polar orbit (values in white). But what is striking is that the high FIP fractionations (Mg/O values) all occur at low to mid latitudes. At high southern latitudes the FIP fractionation, be it in ICMEs or in just ordinary slow solar wind, is clearly less pronounced than it can be at low latitudes. This trend, illustrated by the red triangle surrounding the Mg/O values, is not pronounced, but the strongly FIP fractionated materials including ICMEs seem to avoid the polar regions. This is remarkable, as it appears to indicate a difference in the pre-CME state or onset mechanism of ICMEs.

Filaments are generally believed to have chromospheric composition (Schwenn *et al.*, 1980). The chromosphere is a thin layer of the Sun's atmosphere and is very likely intimately connected with the FIP effect (von Steiger, 1998; Laming and Feldman, 2001). It could be where the FIP effect acts on the solar wind flow, or it could lie beneath that location. Hence it is interesting to investigate filamentary material as a test of FIP-fractionation models. Neukomm (1998) has investigated ICMEs observed with Ulysses and found no evidence of photospheric composition in these ICMEs. This would argue that ICMEs (and the filaments within) are already (FIP) fractionated and certainly do not exhibit photospheric composition. This is borne out by the lowest panel of Figure 1 which shows the Mg/O elemental abundance ratio, a good proxy for the FIP effect. Except for few days at high southern latitudes during solar activity maximum, no solar wind was observed that had not been (FIP) fractionated. The analysis of the few days with unusually low Mg/O is still outstanding. As they do not coincide with periods of unusually low coronal temperature, a filamentary origin seems unlikely.

Some He isotopic anomalies in ICMEs have been reported. In the normal solar wind, the He isotope ratio $^3He^{2+}/^4He^{2+}$ has been determined as $(0.43 \pm 0.02) \cdot 10^{-3}$ (Geiss *et al.*, 1970b), while enhancements of $^3He^{2+}/^4He^{2+} \geq 10^{-3}$ always coincide with ICMEs (Ho *et al.*, 2000). Other isotopic anomalies of heavy elements have not yet been observed, mainly because of the low counting statistics of isochronous time-of-flight mass spectrometers (Wimmer-Schweingruber *et al.*, 1999b).

In summary, the range of variability of elemental abundances in ICMEs is large, both between different events as well as within one single event. It ranges from no compositional signature at all (with respect to the surrounding solar wind) to unusual events with compositions never seen in other contexts.

2.3. Relating Charge-State and Elemental Composition

In a study comprising about 200 ICMEs detected in the near-Earth environment, Richardson and Cane (2004) investigated various compositional signatures as a function of the location relative to the ICME boundaries. Results of this analysis are displayed in Figure 2. Periods with anomalous plasma composition are found to occur in non-cloud (left-hand panel) and in cloud (right-hand panel) ICMEs. Their criteria for "anomalous" composition are summarized in Table I. In general,

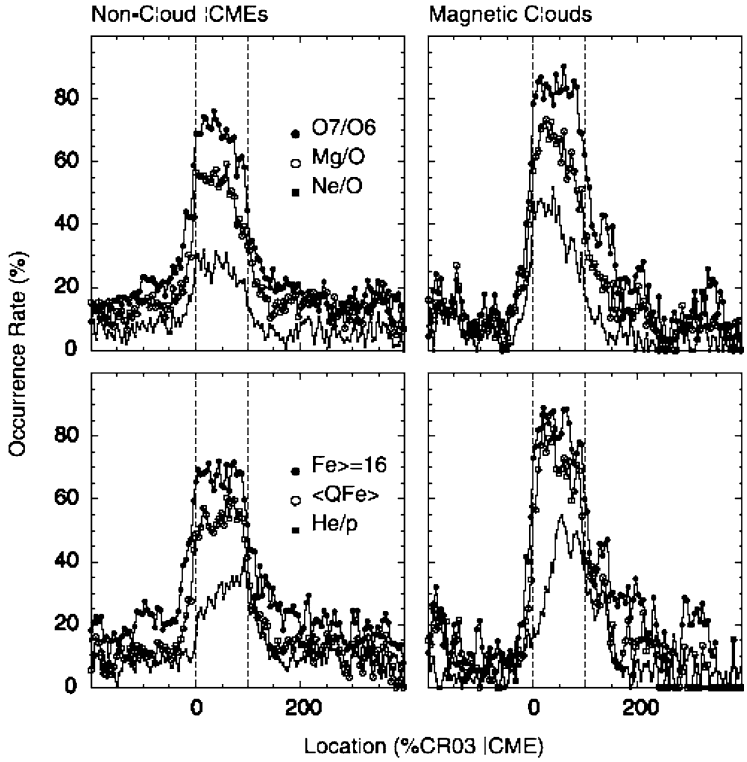

Figure 2. Occurrence rate of periods with anomalous composition for various signatures as a function of time/location with respect to the boundaries of cloud and non-cloud ICMEs. "Anomalous" is defined in Table I. An occurrence rate of 60% means that 60% of all ICMEs (non-cloud or cloud) exhibit that signature. 0% on the x-axis corresponds to the leading edge and 100% represents the trailing edge (From Richardson and Cane, 2004. © American Geophysical Union. Reproduced/modified by permission of American Geophysical Union).

TABLE I

Parameters characterizing "expected" and "anomalous" composition ratios in the solar wind; v is the solar wind speed.

Signature	Normal v-dependence	Anomalous	Reference
O^{7+}/O^{6+}	$3.004 \cdot \exp(-0.00587v)$	$2 \times$ normal	a
Mg/O	$0.491 \cdot \exp(-0.00367v)$	$2 \times$ normal	a
Ne/O	$0.295 \cdot \exp(-0.0017v)$	$2 \times$ normal	a
$Q_{Fe} \geq 16/\sum Q_{Fe,tot}$	$0.292 \cdot \exp(-0.00421v)$	$2 \times$ normal	a
$\langle Q_{Fe} \rangle$	$11.2 - 0.000857v$	$Q \geq \langle Q_{Fe} \rangle + 1$	a
He/p		≥ 0.06	a
$^3He/^4He$		$\geq 10^{-3}$	b

References: (a) Richardson and Cane (2004), (b) Ho *et al.* (2000).

elevated charge states provide higher occurrence rates when compared to elemental abundance ratios. The profiles presented in the top panels suggest a decrease in the occurrence rate of compositional anomalies from the leading to the trailing edge of ICMEs. Even though this may indicate a spatial trend, the possibility of a bias introduced by the ICME expansion and the criteria for selecting the anomalous periods cannot be discarded. Helium enhancements (lower panels) present the opposite behaviour (increasing occurrence rate towards the trailing part of ICMEs), consistent with gravitational settling of helium in the bulk material of coronal streamers (Geiss *et al.*, 1970), potential pre-CME coronal structures. However, the heavier elements Mg and Ne do not appear to be enriched relative to the lighter element oxygen towards the trailing edges of the ICMEs as would be expected in this picture. Their abundance, however, is consistent with fractionation by insufficient proton drag, as is seen in the vicinity of sector boundaries (Wimmer-Schweingruber, 1994) originating in coronal streamers (Borrini *et al.*, 1981).

The similarities in the overall spatial behavior of both elemental and ionic charge-state anomalies relative to the normal solar wind are quite remarkable when one considers the widely different time scales at work. While elemental fractionation processes need to be active for substantial time periods (on the order of days in the Wurz *et al.* (2000) model) in the pre-CME structures, charge states are determined along CME trajectories through the corona (on timescales of hours), and also very likely during the intense energy release associated with CME initiation (Reinard, 2005). Indeed, flare emissions clearly indicate that large amounts of thermal energy are released during the formation of a CME. Evidently, the low-density corona is also affected by this transfer from magnetic to thermal and kinetic energy, which is likely to be associated with magnetic reconnection and, hence, the CME initiation process (Forbes *et al.*, 2006, this volume). Frozen-in ionic charge states may therefore provide one of the most direct measures of the

initiation process, while elemental composition probes pre-CME solar atmosphere conditions.

2.4. Bidirectional Electron Streaming

One of the first signatures used to identify ICMEs on a routine basis is counterstreaming of suprathermal (>80 eV) electron beams, or bidirectional electrons (BDEs) (e.g., Gosling *et al.*, 1987, 1990). Since the solar corona is a nearly continuous source of hot electrons, one normally observes a suprathermal electron beam called the "strahl" (e.g., Pilipp *et al.*, 1987) flowing away from the Sun along heliospheric magnetic field lines that are open (extending from the Sun to infinity). Counterstreaming beams form when field lines are connected to the Sun at both ends. These closed field lines can be either simple loops or coiled loops in flux ropes, the latter as sketched in Figure 2 of Zurbuchen and Richardson (2006, this volume). It is nearly always assumed that field lines closed in this manner arise from CMEs (see section 5 for exceptions).

On the other hand, not all field lines in ICMEs are necessarily closed. Some ICMEs, as identified by other signatures, are devoid of BDEs, and many contain intermittent intervals of BDEs, implying a mix of open and closed fields (e.g., Gosling *et al.*, 1995; Shodhan *et al.*, 2000; Crooker *et al.*, 2004a; Crooker and Horbury, 2006, this volume). Nevertheless, nearly all ICMEs observed within 5 AU of the Sun contain some closed fields and, on average, appear to contain more closed than open fields ($\sim$ 60% in magnetic clouds at 1 AU).

In using BDEs to identify ICMEs by their closed fields, one must avoid counterstreaming events generated on open field lines. Shocks are a well-known source because they accelerate electrons to suprathermal energies. As a result, magnetic connection to shocks beyond the observer can result in a beam of electrons flowing opposite to the electron outflow from the Sun. In the case of Earth's bow shock, this signature can usually be recognized and avoided by estimating whether the spacecraft is magnetically connected using simple geometrical models (e.g., Stansberry *et al.*, 1988). In addition, well away from Earth (say at L1), counterstreaming created by bow-shock connections usually can be distinguished from BDEs in ICMEs by the relatively short (<1 hr) connection duration owing to ever-present fluctuations in field direction. In the case of corotating shocks, electrons backstreaming toward the Sun are usually clear in pitch angle spectrograms because they characteristically stop or start with shock passage (e.g., Gosling *et al.*, 1993). In the case of shocks created by ICMEs, any electrons backstreaming toward the Sun would be found in the sheaths between the shocks and ICMEs (Figure 2 of Zurbuchen and Richardson, 2006, this volume), but few cases have been observed.

Counterstreaming on open field lines can also be generated by focusing and mirroring on field lines connected to regions of elevated magnetic field magnitude downstream of a spacecraft (Gosling *et al.*, 2001). These adiabatic actions create

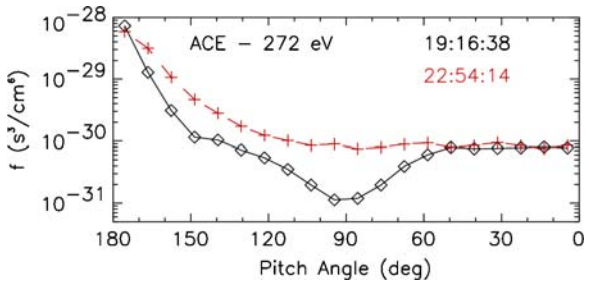

Figure 3. Two pitch angle distributions measured by ACE on 10 January 1999. The single beam at 180° indicates open field lines in both cases, while a depletion at 90° is apparent only in the distribution plotted with diamonds (from Gosling *et al.*, 2001. © American Geophysical Union. Reproduced/modified by permission of American Geophysical Union).

electron pitch angle distributions with a band of depletion centered on 90°. Gosling *et al.* (2001) estimate that depletions are present at least 10% of the time. Close examination of the shape of the pitch angle distribution can help distinguish depletions on open fields from BDEs on closed fields. Depletions produce a dip at 90° in a distribution that peaks either at 0° or 180° and is otherwise flat, as illustrated by the diamond symbols in Figure 3, whereas distributions on closed fields generally peak at both 0° and 180°. This distinction, however, is not always clear. Crooker *et al.* (2004a) report that their estimated average of 55% for closed fields in magnetic clouds at 5 AU is an upper limit and could be as low as 40% owing to mistaking depletions on open field lines for BDEs on closed field lines.

Sometimes counterstreaming suprathermal electrons can be confused with large temperature anisotropies in the core electrons, which commonly occur during periods of low plasma density (Phillips and Gosling, 1990), because at such times the core distribution extends up to energies much higher than 80 eV along the field. Commonly, the temperature parallel to the field is larger than the temperature perpendicular to the field. This sense of anisotropy results in a double field-aligned band of increased intensities in spectrograms at suprathermal energies below about 300 eV, mimicking the closed-field-line signature. These can be distinguished from each other by checking whether the double-banded pattern extends to energies well below 80 eV and if the apparent counterstreaming extends up to energies well above 300 eV.

Attempts to design quantitative routines for objectively selecting BDE events on closed field lines have met with little success. For example, Feuerstein *et al.* (2004) constructed scatter plots of suprathermal electron intensities parallel against antiparallel to the magnetic field, each intensity normalized by the intensity perpendicular to the field, and found no clearly separate BDE population in their plots. Instead, points in BDEs blend in with the unidirectional populations, owing at least in part to the fact that one counterstreaming beam is nearly always stronger than the other. This may reflect different source conditions at the base of each leg of the

closed loops and/or a skewing of closed loops along the Parker spiral, thus biasing spacecraft interception toward one leg of the loop rather than its apex. The intensity of the beam from the base of the intercepted leg is expected to be stronger than the intensity of the beam from the more distant base of the far leg (Pilipp *et al.*, 1987). Other factors that undoubtedly contribute to the spread in BDE points are the effects of 90°-depletions and temperature anisotropies in the core population, as discussed above.

In summary, while BDEs continue to be a widely accepted signature of closed magnetic fields in ICMEs, identifying them in pitch angle spectrograms continues to be a somewhat subjective process.

2.5. Magnetic Clouds

As discussed by Zurbuchen and Richardson (2006, this volume), magnetic clouds are a subset of ICMEs defined at 1 AU by the following criteria (Burlaga, 1991): (1) the magnetic field direction rotates smoothly through a large angle during an interval of the order of one day; (2) the magnetic field strength is higher than average; and (3) the temperature is lower than average. Other large-scale solar wind structures, such as interplanetary sector boundaries, co-rotating interaction regions (CIRs) or post-shock ICME flows, can exhibit any of the above features (e.g., Bothmer and Schwenn, 1992), but the combination of all three appears to be unique to magnetic clouds (e.g., Bothmer and Schwenn, 1998).

Goldstein (1983) introduced the now widely used force-free ($\nabla \times \mathbf{B} = \pm\mathbf{B}$) large-scale cylindrical magnetic flux rope model to explain the magnetic field variations in magnetic clouds. Later studies, however, show that not every cloud fits a force-free, cylindrically symmetric model (e.g., Mulligan and Russell, 2001; Hidalgo *et al.*, 2002; Forbes *et al.*, 2006, this volume).

Bothmer and Schwenn (1998) used Helios 1 and Helios 2 data in order to systematically study magnetic clouds between 0.3 and 1 AU. They found that, during the years 1974 to 1980, 74% of the clouds showed South to North rotations of the magnetic field vector. Using additional observational results for the average properties of prominences (disappearing filaments) and photospheric bipolar regions (sunspots), they explained the dominance of this type of rotation and introduced the solar cycle relationship of the field structure of magnetic clouds shown in Figure 4. The dominance of SN type magnetic clouds in odd cycles and of NS ones in even cycles was thus explained as a consequence of the predominant magnetic polarity of sunspots and bipolar regions in the two solar hemispheres in a given solar cycle, of the average orientation of neutral lines separating them, and of the orientation of filaments (see, also, Bothmer and Rust, 1997). This and related solar imprints on magnetic clouds are discussed further by Forsyth *et al.* (2006, this volume) and Crooker and Horbury (2006, this volume).

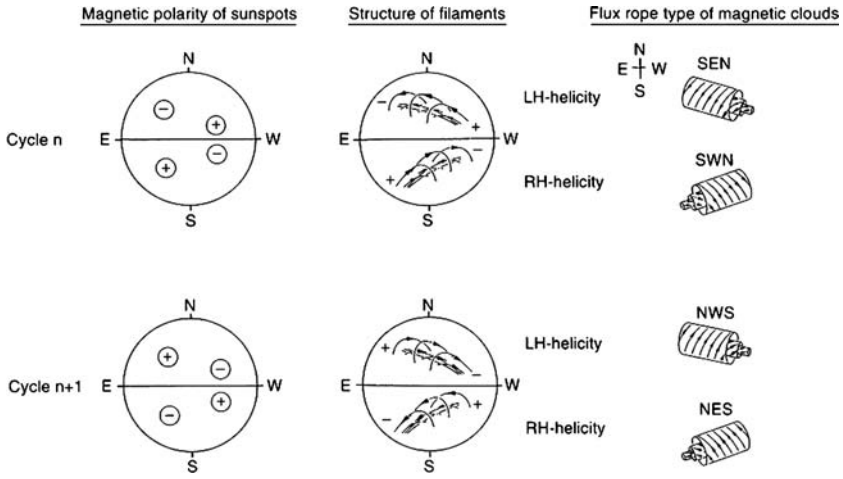

Figure 4. Solar cycle dependence of the magnetic field structure of filaments at the Sun and that of the corresponding magnetic clouds in the interplanetary medium. Adapted from Bothmer and Schwenn (1998). Note that for simplicity the magnetic clouds are oriented horizontally with respect to the ecliptic plane. Furthermore, the "cycle overlap" during the declining phase of the preceeding cycle is not considered here. In this complicated phase the old magnetic polarity is still prominant in near-equatorial regions, while the new polarity emerges at mid to high latitudes.

Recent cloud studies by Huttunen *et al.* (2005) and Wu *et al.* (2003) show that the overall frequency of magnetic clouds varies over the course of the solar cycle but was not in phase with either the sunspot cycle nor the total CME rate during 1996–2002. Richardson and Cane (2004b), however, noted that the total number of near-Earth ICMEs approximately follows the solar cycle and concluded that the fraction of ICMEs that are magnetic clouds varies from roughly 100% near times of solar minimum to about 15% around solar maximum.

2.6. A Case Study: The 2000 Bastille-Day Event

On July 14, 2000, the LASCO coronagraphs on board the Solar and Heliospheric Observatory (SOHO) observed a front-side full halo CME (top right-hand panel of Figure 5) with a speed of $\sim$ 1600 km/s in the plane of the sky at about 11 UT (Lepping *et al.*, 2001). SOHO's solar magnetic field (MDI, lower left-hand panel) and extreme ultraviolet (EIT, lower right) observations and Yohkoh's soft X-ray measurements (upper left) show that the CME originated from a bipolar magnetic region located in the northern solar hemisphere around central meridian. In soft X-rays, a sigmoid structure became prominent near the CME's onset time, indicative of coronal heating. The sigmoid was followed by a post-eruptive arcade (insert in EIT image), an unmistakable signature of CMEs (e.g., Sterling *et al.*, 2000; Tripathi *et al.*, 2004).

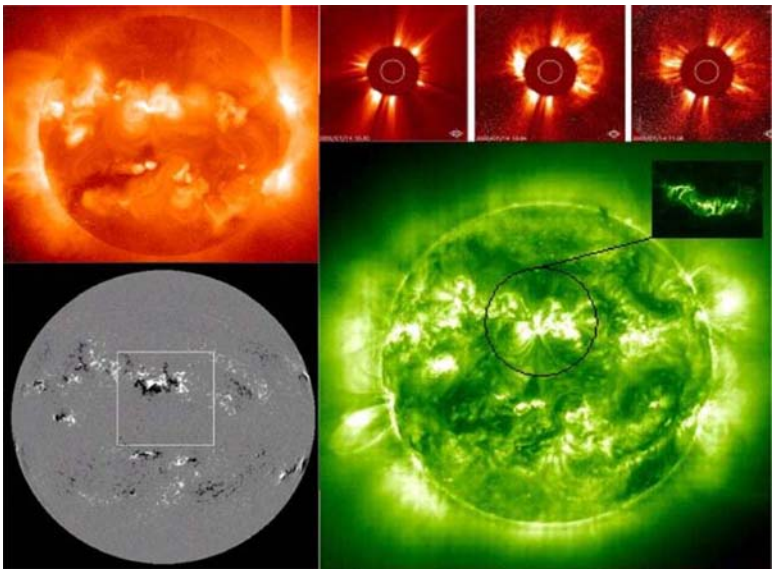

Figure 5. Combined SOHO and Yohkoh observations showing the July 14, 2000 halo CME and its corresponding source regions in the lower corona and photosphere. The EUV post-eruptive arcade demarks the CME source location on the visible solar disk. The square in the lower left-hand panel denotes the bipolar region of origin, the sigmoid structure is seen at the corresponding location in the panel above. The remains of the source region are seen as post-eruptive arcades in the EIT image (lower right). The resulting halo CME is clearly visible in the three LASCO images (upper right) (Adapted from Bothmer, 2003).

The ICME corresponding to the halo CME was detected by several spacecraft stationed near Earth. In-situ data from ACE of this and preceding ICMEs are shown in Figure 6. The top three panels show magnetic field data B, RTN θ_B, and ϕ_B (all from ACE level 2 data), the next three panels show proton data, v_p, T_p, and n_p (SWEPAM data, courtesy R. Skoug and D. J. McComas), and the three bottom panels show composition data (from SWICS). These are the ionic charge-state ratios C^{6+}/C^{5+} and O^{7+}/O^{6+}, average iron charge state, $\langle Q \rangle_{Fe}$, and elemental abundance ratios Mg/O and Fe/O. Because of the high background due to penetrating particles, SWEPAM data has only $\sim$ 30 minute resolution from DOY 196/11:06–198/01:33, and He^{2+} data were unavailable. Halo electron measurements were also not available during 196/02:00–197/23:00 (Smith *et al.*, 2001). The time period shown here was preceded by an interval with two ICMEs. The end of the second of these is labeled *a* in the uppermost panel. The following ICME labeled *b* is indicated by a thin two-ended arrow bounded by two thick vertical dashed lines at 196/17:00 and 197/14:00. It is clearly identified by the low level of fluctuations in B and by the enhanced ionization temperatures in the second half. He/O shows a sharp increase from a low value to a very high value exceeding 200. ICME *b* contained a magnetic cloud indicated by the thick two-ended arrow labeled 1 above the panels and the

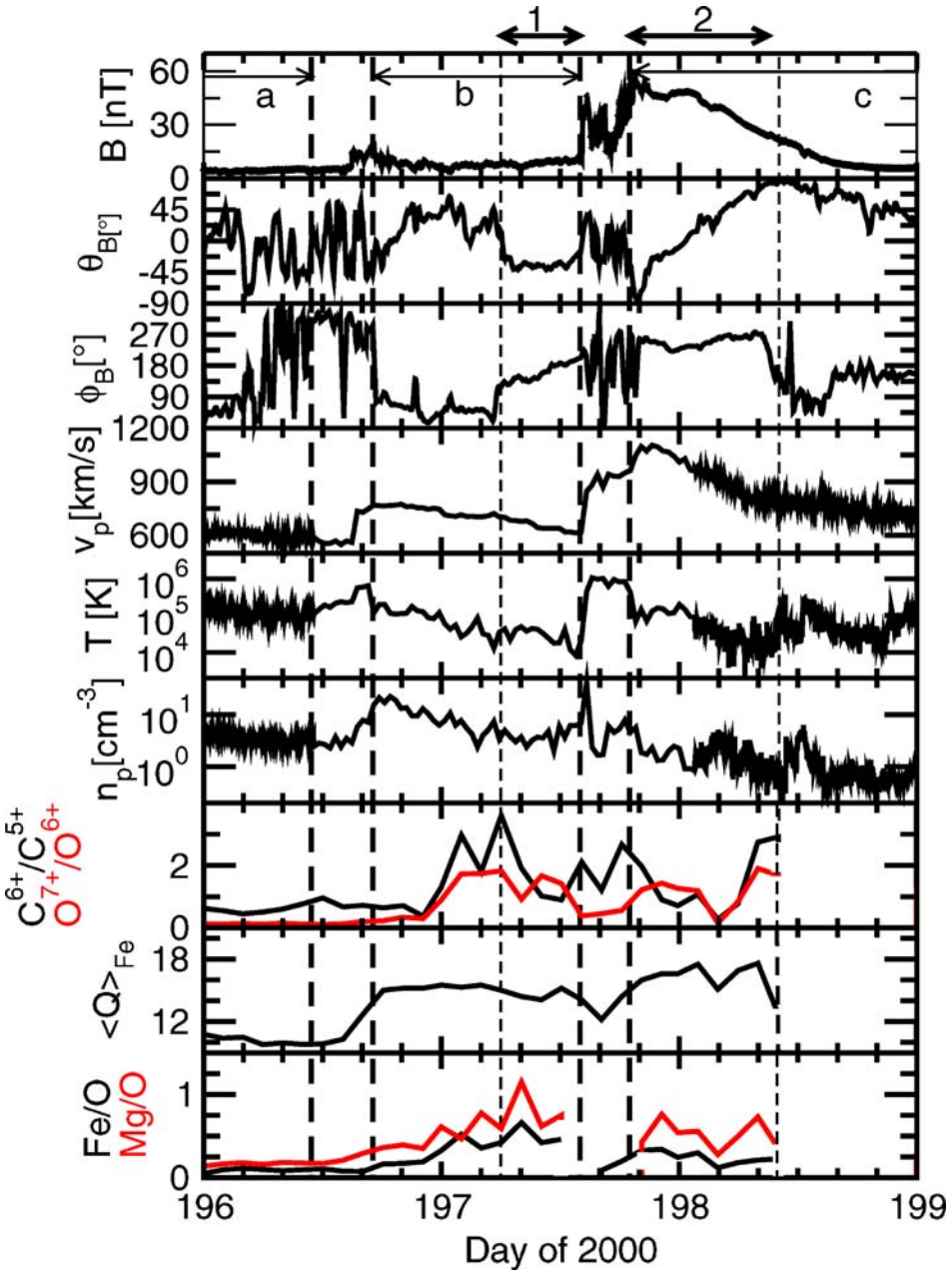

Figure 6. In-situ data from the ACE spacecraft for the ICMEs/magnetic clouds observed on July 14–16, 2000. From top to bottom: B, θ_B, and ϕ_B in RTN coordinates. Proton speed, temperature, and density are from SWEPAM, the lower three panels show charge-state ratios of carbon and oxygen, average iron charge state, and elemental abundances of Fe and Mg relative to O from SWICS. The thick double-ended arrows at the top of the panel denote the magnetic clouds, while the thin lines inside the topmost panel show the ICMEs. ICME c extended beyond the time period shown here.

thin vertical dashed line. It is clearly visible as a systematic rotation in ϕ_B and low proton temperature. Ionization states rose before the onset of the magnetic cloud. ICME *c* started with magnetic cloud 2 (again indicated by a thick double-ended arrow and a thin vertical dashed line marking its end). See Smith *et al.* (2001) for timing information.

ICME *c* corresponds to the halo CME in Figure 5, launched on July 14, 2000, described in the previous paragraph. From the MDI measurements in Figure 5 one may infer that ICME *c* originated from the region of opposite magnetic polarities inside the square, as is generally the case for the source regions of CMEs that can be tracked back to the solar surface (Cremades and Bothmer, 2004). White areas in the MDI image denote magnetic fields pointing away from the solar surface, and black areas denote fields pointing towards the surface. If, inside the square, one drew an arcade of field lines from one polarity to the other and let them expand radially outward and reconnect beneath, one would expect to observe a South to North turning of the magnetic field vector in space. This is the direction of turning predicted according to the classification scheme in Figure 4, and it matches the negative to positive rotation in θ_B in the second panel of Figure 6.

The high magnetic field strength and strong proton speed gradient in the first and fourth panels during cloud 2 in Figure 6 indicate that this cloud was still expanding as it reached ACE. The strong southward B component coincided with the high speed, exceeding 1100 km/s at the leading edge of the cloud, and triggered a large geomagnetic storm on July 15–16, 2000. The depressed proton temperature in the fifth panel together with the high field strength resulted in a low-β structure. The coincident low density seen in the sixth panel, possibly due to the expansion, led to a near sub-Alfvénic flow within magnetic cloud 2 (Smith *et al.*, 2001). In the third panel of Figure 6, magnetic field longitude, ϕ_B, shows large excursions towards the end of ICME *a*, between ICME *a* and *b*, and between magnetic clouds 1 and 2. These field polarity reversals are not unusual (Klein and Burlaga, 1982). ICMEs and magnetic clouds have been found to replace the heliospheric current sheet reversal in several instances (Crooker and Intriligator, 1996; Crooker *et al.*, 1998; Crooker and Horbury, 2006, this volume). In the seventh panel of Figure 6, the He/H ratio increases sharply at the onset of ICME *c*/cloud 2, (not shown, but see Smith *et al.*, 2001) as does O^{7+}/O^{6+}, but less so for C^{6+}/C^{5+}. The oxygen charge states, as well as the average iron charge state in the bottom panel, are highly elevated, corresponding to a source electron temperature of at least 2.5–3 MK. Together with the low in-situ proton temperature, this implies a strong heating at the source with a subsequent rapid cooling of the plasma as it expanded on its way out of the corona into interplanetary space. The similar elemental composition of ICMEs *b* and *c* indicates a common origin. The preceding ICME *a* had a different elemental composition, similar to the slow solar wind, hinting at a different origin. Alternatively, its ejection could have triggered a strong elemental fractionation in the source plasma of ICMEs *b* and *c*.

2.7. Application: The Genesis ICME Detection Algorithm

As an application of the use of in-situ signatures to identify ICMEs, we discuss the ICME detection algorithm used on the Genesis spacecraft. While it does not make use of all the signatures discussed so far, it appears to have worked rather well and is probably one of the best studied algorithms for this task. The primary purpose of the Genesis mission was to measure both the elemental and isotopic compositions of the outer layers of the Sun. To accomplish this, the spacecraft collected samples of the solar wind, which were returned to Earth in 2004 for analysis. To differentiate between different types of wind, collectors were exposed according to an on-board algorithm (Neugebauer *et al.*, 2003; Reisenfeld *et al.*, 2003). The algorithm attempted to distinguish between three fundamental solar wind flows: high-velocity streams emanating from coronal holes (CHs); slower, inter-stream flow (defined as flow observed between successive coronal hole streams); and ICMEs. Here we describe how the real-time, on-board data were used to identify the presence of ICMEs.

It is worth noting several limitations of the technique as implemented for the Genesis mission. First, the primary objective was to provide pristine samples of CH flow, at the expense of contaminating the interstream and CME samples. Second, the array-changing mechanisms had a design requirement of 400 regime changes over the entire mission. Third, only the ion and electron monitors supplied data to the algorithm. A magnetometer, ion mass spectrometer, and energetic particle detectors were not available on Genesis.

The algorithm took as input the following parameters: (1) Solar wind speed (v_p); (2) the ratio of expected proton temperature for normal solar wind to the measured proton temperature (T_{ex}/T_p); (3) the He^{2+}/p ratio ($n_{He^{2+}}/n_p$); and (4) a bidirectional streaming parameter (B_e). The expected temperature T_{ex} was computed as a linear function (Neugebauer *et al.*, 1997), a quadratic function (Burlaga and Ogilvie, 1973) or combination thereof (Lopez, 1987) of v_p, such that T_{ex}/T_p significantly exceeds 1 within CMEs, reflecting their unusually low temperature (Richardson and Cane, 1995). The bidirectional streaming parameter (B_e) was computed from the angular distribution function of suprathermal electrons. Operationally, the algorithm identified the peak count rate (C_{peak}), the minimum count rate ($\pm 90^\circ$ away from this peak, C_{min}), and the count rate 180° away from the peak (C_{180}). If the ratios $C_{\text{peak}}/C_{\text{min}}$ and C_{180}/C_{min} exceeded some threshold, the algorithm assigned a value of 1 to B_e.

Running averages of the solar wind speed, temperature, alpha abundance, and bidirectional streaming parameter were computed over one hour windows. The algorithm began by assessing whether the spacecraft had encountered a forward shock within the last 12 hours. This does not preclude identifying slow CMEs (i.e., CMEs that do not drive a shock); however, the criteria for switching to the CME regime were made more difficult if no shock occurred. Using a simple fuzzy-logic scheme incorporating: (1) $n_\alpha/n_P > 0.06$; (2) $T_{ex}/T_p > 1.5$; (3) $B_e = 1$; (4) the identification of a shock within the last 24 hours; and (5) whether the CME

criteria were met within the last 6 hours, a threshold was set, above which a CME regime is triggered (i.e., the CME array is exposed to the solar wind). Extra safety mechanisms were also built into the algorithm. For example, it was not possible to trigger a change into the CME regime based solely on B_e since connections to CIR-associated and planetary bow shocks can produce a bidirectional electron signature, as discussed in Section 2.4.

Given how difficult it can be for an "expert" to identify a CME (and particularly its boundaries) even when a full complement of data sets is available, one might question how successful such an automated procedure can be. After identifying and fixing a number of problems associated with the algorithm during the initial portion of the mission, the algorithm appears to have performed satisfactorily. The shock-identification portion of the algorithm worked well, and shocks observed at Genesis matched well with those identified by the SOHO spacecraft. Moreover, it is important to remember that the primary goal of the algorithm was not to identify CMEs but rather to exclude CME material from the coronal hole regime. As is discussed in Reisenberg *et al.* (2003), who compared the Genesis regimes with those identified with additional criteria such as solar wind composition from ACE/SWICS, the agreement between the two independent methods was remarkably good.

3. Boundaries and Multiple ICMEs

3.1. Relative Timings and Intercomparison of Signatures

As noted at the beginning of Section 2, the boundary between an ICME and the ambient solar wind might be expected to be a simple tangential discontinuity that encompasses a region with ICME-like signatures. In practice, ICME boundaries are often elusive, ambiguous, or complex. In particular, the various ICME signatures often do not indicate exactly the same boundaries (e.g., Zwickl *et al.*, 1983; Crooker *et al.*, 1990; Neugebauer and Goldstein, 1997; Richardson *et al.*, 2003), presumably since they arise from a variety of phenomena (Zurbuchen and Richardson, 2006, this volume). Plasma boundaries may also be identified within ICMEs.

One case study, by Crooker *et al.* (1990), is shown in Figure 7. They identified 11 magnetic field discontinuities in the vicinity of a magnetic cloud previously identified by Zhang and Burlaga (1988) and bounded by discontinuities 5 and 8. Discontinuities 2, 4, 5 and 7 were determined to be tangential discontinuities and aligned nearly parallel to each other, while others yielded ambiguous results. Discontinuity 1 is the ICME-driven shock. Near the leading edge of the following ICME, the decrease in proton temperature (at discontinuity 2) occurs earlier than the leading edge of the putative magnetic cloud. If the temperature decrease is taken as the true ICME boundary, then there is a distinct region of predominantly eastward magnetic field ($B_y > 0$) inside the ICME prior to the classic magnetic cloud signature (which has a westward field at the leading edge). Discontinuity 5 would

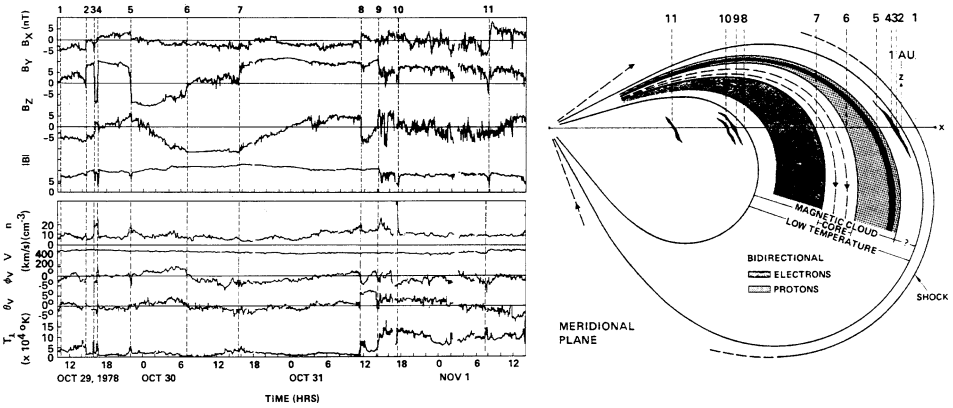

Figure 7. (Left) Magnetic field observations in the vicinity of a magnetic cloud in October, 1978. Discontinuities are numbered. (Right) Interpretation (in the meridional plane) of the structures shown in the left-hand panel and their relationship to BDE and bi-directional energetic ion intervals Crooker *et al.,* 1990. © American Geophysical Union. Reproduced/modified by permission of American Geophysical Union).

then indicate the boundary of flux-rope-like substructure within the ICME rather than the ICME leading edge. In addition, discontinuities 3 and 4 apparently bound a "magnetic hole" (another example may be present at discontinuity 5). Magnetic holes are frequently found near ICME leading edges (Burlaga, 1995). One example discussed by Farrugia *et al.* (2001) was a complex, pressure-balanced structure including a rotational discontinuity and slow shock, with evidence of reconnection between field lines within the ICME. Returning to Figure 7, discontinuities 6 and 7 define the core of the magnetic cloud in which there is little field-line twisting. At the trailing edge, although discontinuity 8 marks the end of the magnetic cloud signature, the proton temperature only recovers fully at discontinuity 9.

Figure 7 also shows a schematic of the ICME structure based on these observations (note that the cloud axis lies approximately perpendicular to the ecliptic, with the mid-plane below the ecliptic). Regions of BDEs and bidirectional energetic ions are also indicated. These predominantly occupy the leading or trailing regions of the magnetic cloud structure, respectively, and both are absent from the cloud core and the low temperature region ahead of the magnetic cloud. Hence, quite different "ICME" regions would be inferred depending on whether the magnetic cloud signature, low proton temperatures, BDEs, or bidirectional ions are considered.

Solar wind composition signatures are now routinely available from instruments such as ACE/SWICS and provide additional clues to the location of ICME boundaries. Although compositional boundaries are often reasonably consistent with those suggested by other signatures, again there may not be total agreement (e.g., cf. Figure 3 of Zurbuchen and Richardson, 2006; Richardson *et al.*, 2003). Boundaries within ICMEs may be associated with substructures of the ICME. For example, Osherovich *et al.* (1999) discuss a magnetic cloud (at Ulysses) which may

be modeled as two intertwined helical flux tubes separated by a region of enhanced plasma pressure. Other case studies of the plasma and magnetic field structures within ICMEs show similar complications. These studies include analysis of the magnetic clouds of 18–20 October, 1995 (e.g., Lepping *et al.*, 1997; Janoo and Farrugia, 1998) and December 23–26, 1996 (e.g., Farrugia *et al.*, 2001; Vasquez *et al.*, 2001).

Multi-spacecraft observations of individual ICMEs also provide unique information on their structure and boundaries. Such observations are rather rare, but several were possible during the Helios 1 and 2 missions. One striking example is an ICME observed in January 1977 by Helios 1 and 2 associated with a filament eruption near E50° relative to the Earth (Cane *et al.*, 1986). Helios 1, located at 0.95 AU and near the filament longitude, observed a shock followed by an ICME

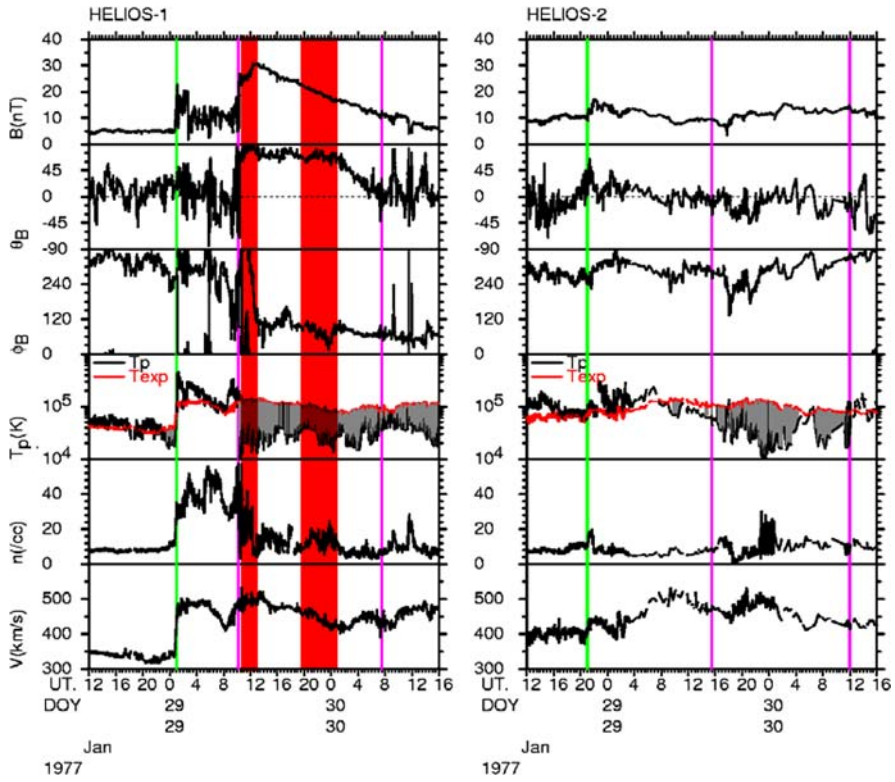

Figure 8. A shock (vertical green line) and ICME (bounded by thin vertical magenta lines) in January 1977 observed by Helios 1 (left) and Helios 2 (right) when the spacecraft were separated by 26° in longitude. The ICME is identified based on the abnormally low proton temperature ($T_p < T_{\exp}$). Note the magnetic cloud-like structure within the ICME at Helios 1 was not encountered by Helios 2, suggesting that it was a substructure of the ICME (adapted from Cane *et al.,* 1997. © American Geophysical Union. Reproduced/modified by permission of American Geophysical Union). Regions in which enhanced levels of He^+ were observed by Schwenn *et al.* (1980) are shaded in red.

with a magnetic cloud signature (Figure 8).At Helios 2, 26° west of Helios 1 at 0.97 AU, the shock was also observed. However, the ICME, indicated by a region of abnormally low proton temperature (and also a cosmic ray depression Cane *et al.*, 1997), lacked a clear cloud-like field signature, suggesting that the magnetic cloud observed at Helios 1 was only a substructure of the ICME. Variations in the other plasma parameters, particularly the density, are also quite different at the two spacecraft. Note also the oppositely-directed magnetic field azimuths (ϕ_B; GSE-coordinates) and that the signature $T_p < T_{\exp}$ persists beyond the magnetic cloud boundary.

3.2. Signatures of Multiple ICMEs

SOHO observations show that CMEs can occur in close spatial and temporal proximity, for example, with several CMEs occurring in succession from the same active region. Thus it is not surprising that some ICMEs are comprised of multiple CMEs, and interactions can occur between ICMEs. Such multiple structures may result in strong heliospheric and geomagnetic disturbances (Burlaga *et al.*, 1987; Bothmer and Schwenn, 1995).

For example, multiple front-side fast halo CMEs were observed during November 24–26, 2000. The corresponding in-situ observations at Earth showed a very complex region of highly-structured plasma shown in Figure 9. Magnetic field and plasma data (from top to bottom $|B|$, θ_B, and ϕ_B are from Wind/MFI, and plasma data v_p, T_p, and n_p are from Wind/SWE). Both data sets were obtained from CDAWeb. The lowest three panels show composition data from ACE/SWICS (O^{7+}/O^{6+}, $\langle Q \rangle_{\mathrm{Fe}}$, and Fe/O and Mg/O from ACE level-2 data). No adjustment for a time lag between ACE and Wind has been made here because the shift would be too small to be visible in this plot. Using a simplified model of four undeformed cylindrical magnetic clouds of variable radius, B-strength and orientation, Wang *et al.* (2002) managed to give a satisfactory explanation of the first two thirds of this region comprising the first three ICMEs/magnetic clouds (marked 1–3 in Figure 9). They appear to have been caused by the first three homologous halo CMEs of that time period. In the last third and for the fourth magnetic cloud (4 in Figure 9), the explanation may be of lesser quality because the last cloud was not caused by one of the homologous CMEs, and the apparent fluctuation (5 in parentheses) cannot be modeled with their approach. On the other hand, the Cane and Richardson (2003) catalogue of ICMEs only contains one ICME in the time period considered here, although they do mention that it could be due to several CMEs. The time period identified by Cane and Richardson is indicated by CR03 above the top panel of Figure 9. It appears to agree better with the compositional data around 08:00 on day 332. Ionization states of oxygen and iron rise to an enhanced level at the onset of the CR03 period, indicating a hot coronal origin. Elemental abundance ratios Fe/O and Mg/O as well as He/H rise dramatically at the onset time, although Cane

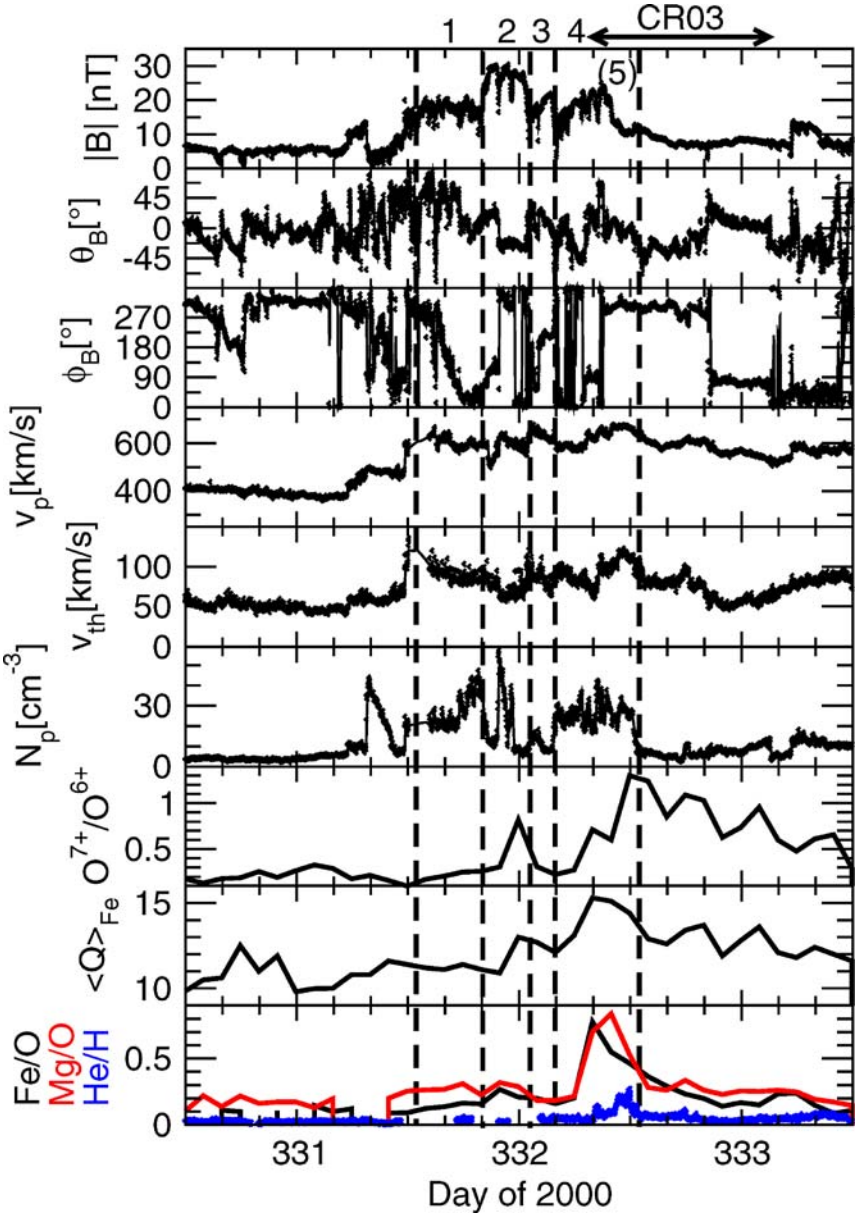

Figure 9. Observations from the November 25, 12:00 UT, to 28 November 2000, 12:00 UT, time period around Earth orbit. From top to bottom: magnetic field strength B, polar and azimuthal field angles θ_B and ϕ_B (in GSE coordinates), bulk solar wind speed v_p, proton thermal speed, $v_{\rm th}$, and proton density N_p, all from Wind (data from CDAWeb). The lowest three panels show compositional data: oxygen charge-state ratio O^{7+}/O^{6+}, average iron charge state, and Fe and Mg to O abundance ratios (data from ACE level 2). Vertical dashed lines denote the borders of the four magnetic clouds (1 – 4) identified by Wang *et al.* (2002). The arrow marked CR03 shows the time period of an ICME identified by Cane and Richardson (2003).

and Richardson did not use these compositional signatures to derive their ICME list (Cane and Richardson, 2003).

Obviously, at times of such complex flows and multiple halo CMEs, it is frequently difficult to relate the flows with specific CMEs. Observations from widely-spaced spacecraft may help to discern the flow structure, such as in the Helios study (previous section) of multiple ICME/magnetic clouds and their interactions with ambient solar wind flows and with each other. Once understood in a more quantitative manner, solar wind composition will also be a very helpful tool in understanding such complex regions in space, much like in the complex corotating interaction regions with multiple stream-interface crossings at high latitudes (Wimmer-Schweingruber *et al.*, 1997,1999).

4. 3-D Structure

4.1. Correspondence to CME Structure

A particularly interesting question is whether one can identify the interplanetary counterparts of the three-part structure of CMEs observed by coronagraphs, i.e., a bright, dense leading edge, low-density (presumably magnetic field-dominated) void, and cool, dense prominence (e.g., Hudson *et al.*, 2006, this volume). The compressed material ahead of the ICME and the ICME proper, respectively, most likely correspond to the first two CME components. Prominence material, which may be indicated by dense plasma with unusually low ion charge states, is only occasionally encountered. However, as discussed in Sections 2.1 and 2.2, Schwenn *et al.* (1980) noted the intermittent presence of He^+ during the ICME observed at Helios 1 and shaded in red in Figure 8, and suggested that this was cold chromospheric material associated with a prominence. Interestingly, Schwenn *et al.* (1980) report He^+ predominantly near the leading edge and centre of the ICME. On the other hand, the prominent He^+ enhancement identified by Burlaga *et al.* (1998) occurred in exceptionally dense plasma ($\leq$185 protons cm^{-3}) at the trailing edge of a magnetic cloud in January 1997. Wurz *et al.* (1998) found dramatic mass fractionation in this filament material. Gloeckler *et al.* (1999) noted that both low and high ion charge states coexisted for extended intervals in the ICME on May 2, 1997. Hence, there appears to be considerable event-to-event variation in the distribution of apparent prominence material that may be due to its 3-D distribution inside the ICME or to true ICME variability.

4.2. Multi-Spacecraft Observations

A fundamental property of an ICME is its extent in helio-longitude and latitude. The longitudinal extents of ICMEs and the related shocks have been examined in several studies of individual ICMEs by multiple, widely-separated, spacecraft. For example, Burlaga *et al.* (1981) identified a magnetic cloud at four spacecraft

(Voyager 2, Helios 1 and 2 and IMP 8) spanning 40° in longitude. The cloud axis was estimated to curve on a scale of ∼0.5 AU at 1 AU. Other ICMEs observed by Helios/IMP 8 were reported by Burlaga *et al.* (1987), Behannon *et al.* (1991), and Bothmer and Schwenn (1996), while Cane *et al.* (1997), noted that remarkably few ICMEs were observed by a pair of spacecraft, even when separated by only ∼ 40° in longitude. They concluded that ICMEs typically extend in longitude only by ∼ 50°, similar to the average *latitudinal* extent of CMEs observed in projection by coronagraphs (e.g., St. Cyr *et al.*, 2000). In such studies, care must be taken to ensure that unrelated shocks/ICMEs at different locations are not erroneously assumed to be part of the same event (e.g., Cane *et al.*, 1991).

Other studies have inferred the longitudinal extents of shocks/ICMEs by observing, at one or more locations, the succession of shocks and ICMEs originating in solar events associated with a major active region as it rotates in longitude due to solar rotation. For example, Figure 10 (Cane and Richardson, 1995) shows a sketch of the ICME and shock configuration inferred from cuts made by the IMP 8 and ISEE 3/ICE spacecraft (located 65°W of Earth) through a sequence of four shocks/ICMEs (numbered 1–4) in October, 1989 that originated in a single active region. The spacecraft trajectories (solid line = shock and ICME encountered; dashed line = ICME not encountered) are drawn relative to the solar event longitude. The ICME width of ±50° from the event location, and the shock width, extending over almost 180°, are consistent with the observations assuming symmetry about the event location. Thus, when the active region is beyond ∼E50° relative to the observing spacecraft, only the western flank of the shock is detected. As the active region moves closer to, then crosses the longitude of the spacecraft, the ICME is detected following the shock. Finally, the active region moves beyond

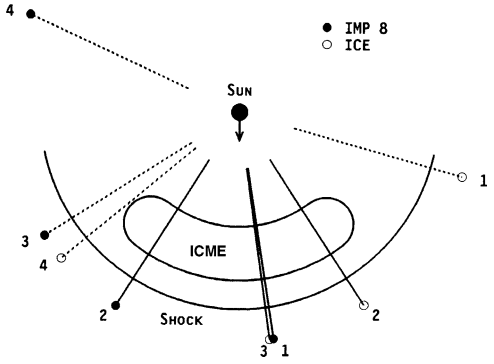

Figure 10. Summary of the trajectories of IMP 8 or ISEE 3/ICE (65°W of Earth) relative to four shocks/ICMEs in October, 1989 (after Cane and Richardson, 1995. © American Geophysical Union. Reproduced/modified by permission of American Geophysical Union), suggesting typical longitudinal widths of nearly 180° and ∼ 100° for the shocks and ICMEs, respectively. (The ICME shape is arbitrary; solid lines indicate trajectories on which the ICME was detected).

$\sim 50^\circ$ west of the spacecraft and the eastern flank of the shock is detected, but not the ICME.

A related approach is a multi-event statistical study examining how the presence or absence of an ICME or shock depends on the longitude of a solar event relative to an observing spacecraft, typically near the Earth (e.g., Borrini *et al.*, 1982; Cane, 1988; Richardson and Cane, 1993; Cane and Richardson, 2003). Such studies again suggest that ICMEs may extend up to $\sim 50^\circ$ in longitude west and east of the solar event location (i.e., a total extent of $\sim 100^\circ$). Cane (1988) concluded from transit speeds to 1 AU that shocks are typically quasi-spherical over at least $\sim 100^\circ$ around the event longitude and extend well beyond the respective ICMEs, as also noted by Borrini *et al.* (1982). In particular, the flanks of shocks from near-limb events may occasionally be detected at Earth. Such studies tend to be dominated by energetic events for which unambiguous associations between interplanetary and solar phenomena can be made. If the related ICMEs are less extended for less energetic solar events, this probably accounts for the smaller size (total width $\sim 50^\circ$) suggested by studies of individual ICMEs.

Thus, ICMEs apparently have typical (full-width) longitudinal extents $\sim 50^\circ$ (which, however, may be larger ($\lesssim 100^\circ$) in particularly energetic events) that are similar to the latitudinal extents of CMEs against the plane of the sky. On the other hand, simple cartoons of flux-rope-like ICMEs (cf. Figure 2 of Zurbuchen and Richardson, 2006) might suggest an ICME structure that is far more extended in the plane of the flux-rope. We conclude that further multi-spacecraft studies (for example of the type performed by Riley *et al.*, 2003) are required to help elucidate the 3-dimensional structure of individual ICMEs and attempt to reconcile current concepts of ICME structure.

It has been estimated that between 20% (solar maximum) and 70% (solar minimum) of all ICMEs contain magnetic flux ropes (Richardson and Cane, 2004b). As such, force-free as well as more sophisticated techniques can provide important insight into their intrinsic properties (see Section 2), provided some basic limitations are taken into account (Riley and Crooker, 2004; Riley *et al.*, 2004). These models are discussed in more detail in Forbes *et al.* (2006, this volume).

4.3. SHOCKS

Shocks can be precursors of ICMEs throughout the heliosphere. ICMEs are often launched from the Sun at speeds greater than the solar wind speed. Since the solar wind is supersonic, a shock must form to allow the accommodation of these two flow regimes. More specifically, a shock will form when the speed difference exceeds the local fast magnetosonic speed. In the inner heliosphere, most shocks are ICME-related (Lindsay *et al.*, 1994), since most corotating interaction region shocks only form beyond 1 AU (Gosling *et al.*, 1976). Roughly 50% of ICMEs are associated with interplanetary shocks (Marsden *et al.*, 1987). These fast forward

shocks propagate through the ambient solar wind ahead of the ICME. Spacecraft in the solar wind will first see the shock, then the region of shocked, compressed plasma and magnetic field called the sheath, and finally the ICME plasma itself (see Figure 2 of Zurbuchen and Richardson, 2006, this volume). Thus, ICME-driven shocks, while not a true signature of the ICME proper, are useful indicators of the possible presence of a following ICME and can be used as such successfully, e.g., in the Genesis algorithm (Section 2.7).

Some high-latitude ICMEs observed by Ulysses are bounded by forward-reverse shock pairs. Gosling *et al.* (1994) suggested that these ICMEs are "overexpanding," meaning that the internal ICME pressure is higher than that of the ambient solar wind. The higher pressure drives expansion into both the leading and trailing solar wind and thus produces shocks and sheaths on both the leading and trailing sides of the ICME. An alternate explanation (Manchester and Zurbuchen, 2006) is that the reverse shock in these events results from the bimodal speed structure of the solar wind near solar minimum, with slow flow at low-latitudes and fast flow at high latitudes. In front of the ICME the slow solar wind is deflected to higher latitude, and behind the ICME the fast flow is deflected to lower latitudes; the collision of these deflected flows results in the formation of a reverse shock.

When data quality is sufficient, the shock normal and the shock speed can be determined. This information helps reveal which part of the ICME is observed; shock normals are radial at the nose of the ICME and rotate away from the Sun-nose direction toward the flanks (Szabo *et al.*, 2001). Numerous methods of determining the shock normal are in the literature. Kasper (2002) used many different methods to determine the shock normal and speed at multiple spacecraft. He then tested the prediction from each model for the time of shock arrival at the downstream spacecraft with the actual shock-arrival time. He found that the Rankine-Hugoniot methods are most accurate.

Comparison of shock normals from multiple spacecraft shows that shocks are not always planar even on the scale of Earth's magnetosphere. Deformations in the shock surface can arise both from asymmetries in the internal structure of the ICME and in the ambient solar wind into which the ICME propagates (Russell *et al.*, 1983; Szabo *et al.*, 1999). Szabo *et al.* (2001) show that even shocks preceding magnetic clouds, which are large coherent structures, show this non-planarity. They find that larger, faster magnetic clouds have more planar shocks than smaller, slower magnetic clouds. The shocks flare away from the cloud's central axis, as expected.

The direction of the magnetic field in the ambient solar wind also influences the geo-effect of an ICME. The sheath regions, comprised of shocked solar wind, have high densities and magnetic fields which may be deflected out of the ecliptic by draping around the ICME (McComas *et al.*, 1989a). The compressed and possibly deflected magnetic field in the sheath make the sheath an important contributor to space weather (e.g., Huttunen *et al.*, 2005). If the shock is perpendicular, the compression of the magnetic field is especially strong. Hence nearly perpendicular

shocks have a much larger probability of driving intense geomagnetic storms than more parallel shocks (Jurac *et al.*, 2002).

4.4. SHEATH PLANARITY

It has long been known (Gosling and McComas, 1987) that compression of the solar wind plasma can lead to the magnetic field being draped around the ICME. This draping of magnetic field lines into the plane of compression within the sheath may lead to the formation of a "planar magnetic structure" (PMS). Planar magnetic structures are extended regions where magnetic field vectors, although of variable direction, lie within a common plane. They were first identified by Nakagawa *et al.* (1989), who suggested various mechanisms for their formation. Neugebauer *et al.* (1993), in a systematic study of PMS events, showed that many of them occurred in the sheath preceding an ICME, a result that is consistent with their generation by the compression of the upstream interplanetary magnetic field lines into a plane.

Clack *et al.* (2000) discussed the planarity of magnetic field lines due to compression within co-rotating interaction regions (CIRs). They pointed out that, since the plane in which the field lines lie is the same as the plane in which the stream interface lies, the orientation of the CIR can be estimated from this PMS plane. The minimum variance direction of the sheath magnetic field vectors should lie along the normal to the PMS plane, making its orientation straightforward to determine using this method. Jones *et al.* (2002) argued that the same effect should be present in the sheaths of ICMEs if they are travelling significantly faster than the preceding solar wind plasma, a scenario that is shown schematically in Figure 11. Therefore, they argued, it is possible to deduce the orientation of the local edge of an ICME from the orientation of the PMS.

Jones *et al.* (2002) showed that it is possible to estimate the position of a spacecraft (in this case Ulysses) relative to the centre of the ICME using PMS analysis.

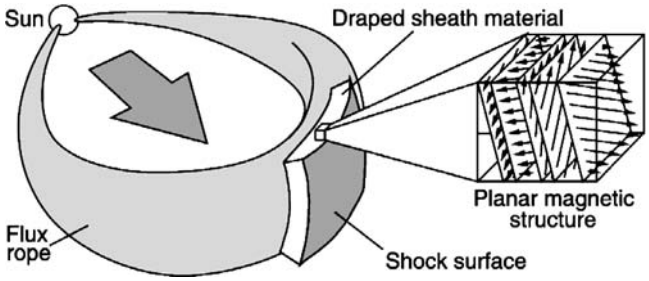

Figure 11. A fast-moving ICME compresses the solar wind ahead of it, leading to magnetic fields draped along this surface: a planar magnetic structure. The normal to this plane provides an estimate of the local orientation of the ICME (from Jones *et al.*, 2002. © American Geophysical Union. Reproduced/modified by permission of American Geophysical Union).

Their results agreed well with those resulting from flux rope fits to the magnetic field profile within ICMEs themselves. This suggests that this technique is a reliable estimator of the orientation of the local edge of the ICME and so could be used with data from several widely-separated spacecraft to estimate the global structure of an event or to determine the orientation of events without clear flux rope signatures.

4.5. Flow Deflections

Gosling *et al.* (1987b) reported flow deflections in the sheath of ICME-driven shocks and also in the ICME itself. In 17 of their 19 investigated shock events, an eastward deflection of the ICME was observed, with an average deflection angle of 3 degrees, corresponding to transverse velocities around 25 km/s. They usually observed an opposite flow deflection in the compressed or shocked ambient plasma ahead of the ICME. They interpreted this systematic pattern as a consequence of the magnetic pressure that builds up ahead of the ICME as the ambient magnetic field is draped around it on its western flank.

Owens and Cargill (2004) further established that, of intervals of non-radial solar wind flow (transverse velocity components >50 km/s) observed by ACE between 1998 and 2002, approximately one third occurred in regions upstream of fast ICMEs listed by Cane and Richardson (2003). The mean value of the maximum transverse flow component in the sheath regions of all fast ICMEs in the survey was of the order of 100 km/s.

In principle the magnitude and direction of these non-radial flows should be related to the shape and orientation of the ICME surface and its speed relative to the ambient solar wind flow. Specifically, for a spacecraft encounter passing through the axis of an ICME, where the axis runs through the length of the loop that is assumed to comprise the ICME, the flow deflection would be expected to be axis-aligned if it weren't for the built-up magnetic pressure of the draped IMF. Moreover, as the interception point of the spacecraft with the ICME moves away from the axis, the flow deflections should develop increasing velocity components perpendicular to the axis. Owens and Cargill (2004) report that typically the non-radial flows in ICME sheath regions are highly structured, containing both discontinuities and gradual rotations. However, for a subset of five events from the above survey where the upstream flow was relatively uniform, they were able to compare the flow deflections with the spacecraft position relative to the ICME axis estimated by variance analysis. They found a general consistency with the pattern of deflections relative to the axis suggested above. This suggests that there is merit in further exploring the possibility of using these deflected flows to make inferences about which part of an ICME a spacecraft is encountering and about the shape of the ICME leading edge and ellipticity of its cross section.

4.6. Energetic Particles and BDEs

The global magnetic structure of ICMEs has been a subject of much debate for a long time (e.g., Morrison, 1954; Cocconi *et al.*, 1958; Gold, 1959). Tongue, bottle, bubble, and connected or disconnected configurations have been proposed (Alexander *et al.*, 2006, this volume). Suprathermal particles serve as tracers of magnetic field lines, providing information on the global configuration of ICMEs. They serve as a tool for discerning between these different ICMEs topologies due to their small gyroradii, great speed and large particle scattering mean free paths in the smooth magnetic fields typical of ICMEs (e.g., Richardson, 1997; Crooker and Horbury, 2006, this volume; Klecker *et al.*, 2006, this volume). Even particles with very high energy, the galactic cosmic rays, are affected by ICMEs. Their intensity is observed to drop inside ICMEs, resulting in Forbush decreases (Cane and Lario, 2006, this volume; Klecker *et al.*, 2006, this volume).

For example, as discussed in section 2.4, bidirectional suprathermal electrons (BDEs, $\sim$100 eV) counterstreaming along magnetic field lines usually indicate that both ends of these field lines connect back to the corona. Earlier papers included the possibility that the field lines form a closed loop, entirely disconnected from the Sun (e.g., Montgomery *et al.*, 1974; Bame *et al.*, 1981; Gosling *et al.*, 1987a), but this is an unlikely extension of two-dimensional thinking. BDEs have also been used to explore magnetic cloud (MC) field polarities. If the dominant electron flow is away from the footpoint closer to the spacecraft, the relative directions of the field and electron flow indicate the field polarity, which should be constant during the magnetic cloud encounter assuming a single flux rope configuration. However, Kahler *et al.* (1999) found changes in polarity which cannot be explained by a single flux rope.

The streaming direction and the flux of electrons may vary extensively throughout a BDE event (e.g., Crooker *et al.*, 1990; Bothmer *et al.*, 1996; Shodhan *et al.*, 2000), indicating that connection of the magnetic field lines to the Sun is patchy. Shodhan *et al.* (2000) found a considerable variability in the duration of BDE events inside magnetic clouds and concluded that "magnetic clouds comprise a random mix of intertwined volumes of magnetically open and closed field lines".

Larson *et al.* (1997) used $\sim$0.1–100 keV electrons to deduce the magnetic topology, field line length and connectivity of a magnetic cloud observed by the WIND spacecraft. Figure 12a, panels A, B and C, show the magnetic field strength and polar and azimuthal angles. A clear rotation of the magnetic field vector is observed, characteristic for MCs. Solar wind speed and density are shown in panels D and E, respectively. Electrons streaming away from the Sun are displayed in panel F and in an energy vs. intensity (relative to quiet-time values) vs. time format in panel G. Several impulsive solar events can be seen above 20 keV. The faster electrons arrive earlier, as expected for injection at the Sun. The onset of each impulsive electron event coincides with a type III radio burst (panel H), which in turn is associated with a flare onset. Pitch angle distributions of 118 eV and 290 eV electrons are shown

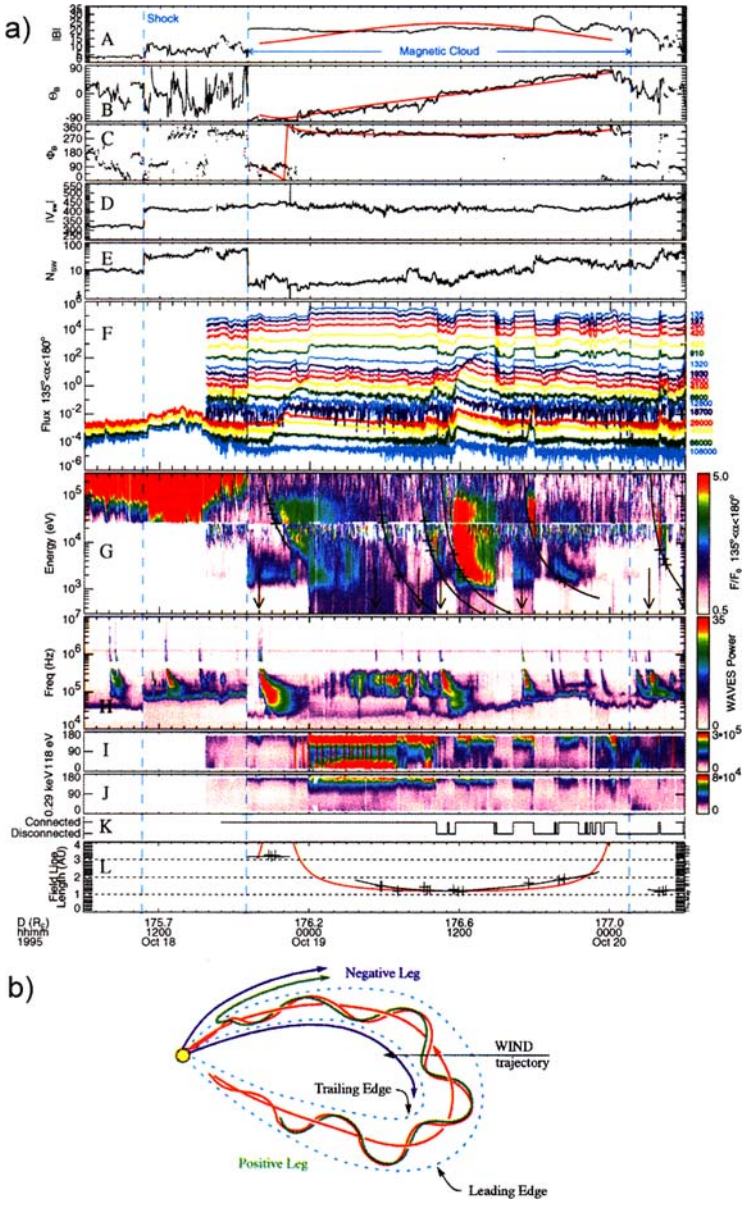

Figure 12. (a) Magnetic field, solar wind plasma, energetic electron, and radio observations from the Wind spacecraft during a magnetic cloud in October 1995; (b) schematic picture of possible topology (from Larson *et al.,* 1997. © American Geophysical Union. Reproduced/modified by permission of American Geophysical Union).

in panels I and J, respectively. BDEs in the 118 eV electrons (starting at ∼0000 UT on October 19) indicate regions with both ends of the field lines connected back to the Sun. After ∼0700 UT on October 19, the electrons are generally unidirectional, indicating magnetic connection to the corona along only one leg of the cloud. Also observable (panels I, J) are many dropouts in the electron fluxes, indicating possible disconnection from the corona (McComas *et al.*, 1989b). This can be also seen in panel K. Field line length in the assumed flux rope form (panel L) is determined from the onset time of the type III bursts and the travel time of these electrons from the Sun. The length varies from ∼3 AU near the leading edge of the MC to $\gtrsim$1 AU near the center and is consistent with a flux rope configuration – the red line shows values expected for a model flux rope. Figure 12b illustrates the cloud topology. It shows intertwined magnetic field lines connected to the Sun at both ends, at one end, and completely disconnected, as proposed earlier by Gosling *et al.* (1995).

Bidirectional energetic particle flows similar to those in suprathermal electrons were first reported for solar energetic particles by Rao *et al.* (1967) and again suggest the presence of magnetic field loops rooted at the Sun. While early papers on bidirectional electron and proton events within ICMEs argued in favour of a disconnected plasmoid topology (Gosling *et al.*, 1987a; Marsden *et al.*, 1987), rapid solar particle event onsets observed by spacecraft located inside ICMEs (e.g., Kahler and Reames, 1991) argue in favour of the interpretation that ICME magnetic lines are rooted at the Sun. If disconnected plasmoids exist, most likely they form through reconnection between open coils and open field lines (step 3 in Figure 3b of Crooker and Horbury, 2006, this volume) and would be devoid of suprathermal electrons. Richardson *et al.* (1991) and Richardson and Cane (1996) noted that occasionally particles from normally poorly-connected eastern solar events arrived promptly in the vicinity of Earth along ICME field lines, also favouring the magnetic bottle configuration. In a study of 13 magnetic clouds detected by the Wind spacecraft, Mazur *et al.* (1998) detected impulsive flare particles in 4 of them. On the other hand, at greater distances from the Sun, Rodriguez *et al.* (2004) found no indication of impulsive electron onsets inside any of 40 magnetic clouds detected by the Ulysses spacecraft. They concluded that if the footpoints are still anchored back at the Sun, then the mechanisms accelerating the particles cannot be continuous from the time of the eruption to the time the MCs reach Ulysses.

Attempts have been made to obtain information on ICME topology using the velocity dispersion of energetic bidirectional ions, since stronger bidirectional fluxes might be expected with increasing particle energy (decreasing time to reach the loop feet) (e.g., Marsden *et al.*, 1987), but (Marsden *et al.*, 1985) and Rodriguez-Pacheco *et al.* (2003) found no such energy dependence. Moreover, in a case study of a cloud for which the flux-rope topology of Hidalgo *et al.* (2002) was assumed, Rodriguez-Pacheco *et al.* (2003) found no agreement with the expectation that, for a given particle energy, the bidirectional fluxes should be stronger at the cloud centre, where distance to the Sun is shortest. Almost the opposite pattern was found.

These authors concluded that mirroring at the cloud feet was not the cause of the bidirectional fluxes. Instead, they suggested that the particles exhibiting bidirectional flows in this event were accelerated at the shock ahead of the cloud and were injected into the ICME as a bidirectional flow. Furthermore, Popecki *et al.* (2001) analysed events in which the presence of particles showing impulsive characteristics was related to shock acceleration in interplanetary space, and not to a possible connection to a flaring region. Thus, the origin of bidirectional ion fluxes in ICMEs is still an open question.

In summary, there is considerable evidence from energetic particle observations that ICMEs consist primarily of a mix of magnetic loops or coils with one or both feet connected back to the Sun. On the other hand, the presence of disconnected plasmoids cannot be ruled out, and open questions remain regarding the interpretation of bidirectional ion signatures.

4.7. Trailing Velocity Increases

Of a more speculative nature, MHD models of flux rope initiation and evolution have been used to predict or verify observational signatures of the reconnection process occurring under the erupting flux rope (Riley *et al.*, 2002; Webb *et al.*, 2003). In particular, Riley *et al.* described how jetted outflow, driven by post-eruptive reconnection underneath the flux rope, would manifest itself as a speed enhancement trailing the ICME, and may remain intact out to 1 AU and beyond. They presented an example of a magnetic cloud with precisely these signatures and showed that the velocity perturbations are consistent with reconnection outflow. This may suggest that other velocity enhancements or unusual composition observed behind magnetic clouds are signatures of such reconnection and, in some cases, may not be associated with prominence material as has previously been suggested, although further analysis of in-situ observations is required to substantiate these tentative conclusions.

5. Other Solar Wind Transients

While ICMEs are the most conspicuous transient structures in the solar wind, they appear to be at one end of a continuum of transient structures that scale down to smaller size and/or to quieter, quasi-steady outflows. In the former category and closest in structure to ICMEs are the small flux rope structures identified by Moldwin *et al.* (1995, 2000). These occur on closed field lines, as signaled by BDEs, and contain the field signatures but not the low temperatures common to magnetic clouds. Moldwin *et al.* (2000) propose that the small flux ropes are created by reconnection in the solar wind rather than back at the Sun.

Other transient signatures, like ICMEs (see Forsyth *et al.*, 2006, this volume), tend to be associated with boundaries between sectors of opposite magnetic polarity, as suggested by Crooker *et al.* (1993), and with the highly variable slow wind in which the sector boundaries are imbedded. For example, large-scale magnetic field inversions immediately adjacent to sector boundaries, deduced from suprathermal electron measurements, have been interpreted in terms of quasi-steady outflows of quiet loops opened by interchange reconnection (Crooker *et al.*, 2004b). When a field line in the leg of a closed loop reconnects with an open field line, it creates a new open field line in which what was originally the leg of the loop becomes a segment that turns back toward the Sun, forming an inversion. The configuration is the same as that illustrated for opening closed fields in ICMEs in Figure 4b of Crooker and Horbury (2006, this volume) except that for inversions adjacent to sector boundaries the configuration must be represented in three dimensions. Crooker *et al.* (2004b) analyzed eight inversions with durations comparable to those of ICMEs. They found that some recurred from one rotation to the next and that a few displayed ICME signatures, most of a marginal nature. They suggest that the inversions may be the heliospheric counterparts of the quiet outflows of loops from active regions reported by Uchida *et al.* (1992).

Smaller-scale transient structures associated with sector boundaries are high-beta heliospheric plasma sheets. At first these were thought to be steady-state structures enveloping the heliospheric current sheet (Winterhalter *et al.*, 1994), which ideally constitutes the sector boundary. Crooker *et al.* (2004c), however, have found that plasma sheets are highly variable. Using suprathermal electron data to distinguish true sector boundaries from local current sheets created by field inversions, they found that plasma sheets are often missing at sector boundaries, sometimes owing to adjacent field inversions covering a wide range of scale sizes, and that plasma sheets often envelop local current sheets away from sector boundaries. Following (Wang *et al.*, 1998, 2000; Crooker *et al.*, 2004c) conclude that the heliospheric plasma sheet may consist entirely of transient plasma sheets and that these may be the heliospheric counterparts of the plasma blobs observed by coronagraphs to emanate from the tips of helmet streamers. If the blobs are released by interchange reconnection, as Wang *et al.* (1998, 2000) suggest, then interchange reconnection may be responsible for the inversions that create local current sheets in some plasma sheets.

Two additional observed patterns deserve mention as possible non-ICME transients: extremely low-density events and radial-field events. Like large-scale field inversions, low-density events can be recurrent, but they have the same kinds of pressure profiles as ICMEs, with magnetic field pressure dominating plasma pressure (Crooker *et al.*, 2000). These characteristics suggest a quiet but transient origin associated with sector boundaries. In radial field events (e.g., Jones *et al.*, 1998), the magnetic field deviates significantly from the Parker spiral toward a direction pointing radially toward or away from the Sun. Unlike the transients discussed above, which are attributed to outflows of spatial structures, radial events have

been ascribed to temporal events, sudden changes in speed at the base of magnetic flux tubes (Gosling and Skoug, 2002; Neugebauer and Liewer, 2003; Wang *et al.*, 2003).

6. Conclusions and Discussion

As has become clear in this chapter, identifying ICMEs in situ is not straightforward. The key problem is that there is no single signature or a combination of signatures that is a foolproof ICME identifier. Different identification methods yield different results and are generally intermittent. The reason for this unsatisfactory state is unclear. Are ICMEs very inhomogeneous, are they individual entities from their onset, are they influenced strongly and differently by their evolution and propagation? These questions are especially important when trying to establish ICME boundaries. While CME boundaries appear reasonably sharp in white-light images, this is not at all the case for ICME boundaries. Why are they often elusive or ambiguous?

This report has clearly shown the potential of composition measurements in identifying ICMEs, but also in investigating their origin and possibly even their evolution and propagation through the solar corona and interplanetary space. We are beginning to understand the richness of elemental abundance and charge-state information, but several questions still remain.

Why is the range of compositional signatures so large? Why do they range from no signature in high-latitude ICMEs to otherwise unseen compositional oddities in a few selected ICMEs? Why are high-latitude ICMEs so different from low-latitude ones, at least compositionally? Is it due to a difference in the pre-CME state or in the onset/initiation mechanism? What is the relationship between ionic charge states and the CME initiation process, and how do we interpret mixed high and low charge states in the same bulk plasma? What leads to the He accumulation in the CMEs that we measure as He abundance enhancements in ICMEs?

The magnetic topology of ICMEs has long been a key in-situ signature for ICME identification. Both magnetic field and bidirectional electron measurements have allowed us to understand the global topology of ICMEs in some detail. Nevertheless, several puzzles remain. Remarkably, not all ICMEs are observed as flux ropes, as theory would predict. Is this simply due to an observational bias, or do ICMEs not necessarily need to be flux ropes? In either case, why does the fraction of magnetic clouds among all ICMEs vary with the solar cycle? While nearly all ICMEs within 5 AU contain some closed fields, somewhat less than half of the field lines within a typical ICME appear to be open, if the intermittency of bidirectional electrons is an indicator for a mix of open and closed fields. Where do these open field lines connect to? When and where do they disconnect? The still unclear magnetic connection of ICMEs with the Sun and the ambient solar wind must somehow be

related to the origin of bidirectional ion fluxes observed in the interiors of ICMEs. We don't understand how.

Doubtlessly, some of the questions mentioned above will be addressed by the upcoming STEREO mission, which, in combination with other assets such as SOHO, Wind, and ACE will allow us to study the inhomogeneity and case-by-case variability of ICMEs in much more detail than previously possible. Nevertheless, the key to understanding the relation between ICMEs and CMEs, and thus ultimately understanding ICME signatures, lies in going closer to the Sun and studying them with a fleet of spacecraft with modern instrumentation such as envisioned with the Solar Orbiter and Sentinels missions.

Acknowledgements

This work was supported, in parts, by the Deutsche Forschungsgemeinschaft DFG. We thank the convenors for organizing a series of three stimulating workshops and the International Space Science Institute, ISSI, for hosting the final one.

References

Alexander, D., Richardson, I. G., and Zurbuchen, T. H.: 2005, *Space Sci. Rev.*, this volume, doi: 10.1007/s11214-006-9013-1.

Antiochos, S. K.: 1998, *Astrophys. J.* **502**, L181.

Bame, S. J., Hundhausen, A. J., Asbridge, J. R., and Strong, I. B.: 1968, *Astro J.* **73**, 55.

Bame, S. J., Asbridge, J. R., Feldman, W. C., Fenimore, E. E., and Gosling, J. T.: 1979, *Sol. Phys.* **62**, 179.

Bame, S. J., Asbridge, J. R., Feldman, W. C., Gosling, J. T., and Zwickl, R. D.: 1981, *Geophys. Res. Lett.* **8**, 173.

Behannon, K. W., Burlaga, L. F., and Hewish, A.: 1991, *J. Geophys. Res.* **96**, 21,213.

Bothmer, V.: 1999, *Solar Wind 9 Conference Proc.*, Published by American Institute of Physics (AIP), p. 119.

Bothmer, V.: 2003, in: A. Wilson (ed.), *Proc. ISCS 2003 Symp., Solar Variability as an Input to the Earth's Enviornment*, **ESA SP-535**, 419.

Bothmer, V., and Schwenn, R.: 1992, *Solar Wind Seven*, Pergamon, Oxford, p. 151.

Bothmer, V., and Schwenn, R.: 1995, *J. Geomagn. Geoelectr.* **47**, 1127.

Bothmer, V., and Schwenn, R.: 1996, *Adv. Space Res.* **17**, 319.

Bothmer, V., and Rust, D. M.: 1997, in: *Proc. of AGU Conf. on Coronal Mass Ejections: Causes and Consequences*, American Geophysical Union Geophys. Monogr. Series, p. 139.

Bothmer, V., and Schwenn, R.: 1998, *Ann. Geophys.* **16**, 1.

Bothmer, V., *et al.*: 1996, *Astron. Astrophys.* **316**, 493.

Borrini, G., Wilcox, J. M., Gosling, J. T., Bame, S. J., and Feldman, W. C.: 1981, *J. Geophys. Res.* **86**, 4565.

Borrini, G., Gosling, J. T., Bame, S. J., and Feldman, W. C.: 1982, *J. Geophys. Res.* **87**, 4365.

Burlaga, L.: 1988, *J. Geophys. Res.* **93**, 7217.

Burlaga, L. F.: 1991, in: R. Schwenn and E. Marsch (eds.), *Physics of the Inner Heliosphere* II, Springer-Verlag, Berlin, Heidelberg, p. 1.

Burlaga, L. F.: 1995, *Interplanetary Magnetohydrodynamics*, Oxford University Press, New York and Oxford.
Burlaga, L. F., and Ogilvie, K. W.: 1973, *J. Geophys. Res.* **78**, 2028.
Burlaga, L. F., and Behannon, K. W.: 1982, *Sol. Phys.* **81**, 181.
Burlaga, L. F., and Behannon, K. W.: 1987, *J. Geophys. Res.* **92**, 5725.
Burlaga, L. F., Sittler, E., Mariani, F., Lazarus, A., Schwenn, R.: 1981, *J. Geophys. Res.* **86**, 6673.
Burlaga, L. F., Behannon, K. W., and Klein, L. W.: 1987, *J. Geophys. Res.* **92**, 5725.
Burlaga, L., Fitzenreiter, R., Lepping, R., Ogilvie, K., Szabo, A., Lazarus, A. *et al.*, 1998, *J. Geophys. Res.* **103**, 277.
Cane, H. V.: 1988, *J. Geophys. Res.* **93**, 1.
Cane, H. V., and Richardson, I. G.: 1995, *J. Geophys. Res.* **100**, 1755.
Cane, H. V., and Richardson, I. G.: 2003, *J. Geophys. Res.* **108**(4), 1156, doi:10.1029/2002JA009817.
Cane, H. V., and Lario, D.: 2006, *Space Sci. Rev.* this volume, doi: 10.1007/s11214-006-9011-3.
Cane, H. V., Kahler, S. W., and Sheeley, N. R., Jr.: 1986, *J. Geophys. Res.* **91**, 13321.
Cane, H. V., Richardson, I. G., and Harvey, K.: 1991, *J. Geophys. Res.* **96**, 19525.
Cane, H. V., Wibberenz, G., and Richardson, I. G.: 1997, *J. Geophys. Res.* **102**, 7075.
Clack D., Forsyth, R. J., and Dunlop, M. W.: 2000, *Geophys. Res. Lett.***29**(5), 625.
Cocconi, G., Gold, T., Greisen, K., Hayakawa, S., and Morrison, P.: 1958, *Nuovo Cimento* **8**, 161.
Cremades, H., and Bothmer, V.: 2004, *Astron. Astrophys.* **422**, 307.
Crooker, N. U., Gosling, J. T., Smith, E. J., and Russell, C. T.: 1990, in: C. T. Russell, E. R. Priest and L. C. Lee (eds.), *Physics of Magnetic Flux Ropes*, Geophys. Monogr. Ser. Vol. 58, AGU., Washington D.C., p. 365.
Crooker, N. U., Siscoe, G. L., Shodhan, S., Webb, D. F., Gosling, J. T., and Smith, E. J.: 1993, *J. Geophys. Res.* **98**, 9371.
Crooker, N. U., and Intriligator, D. S.: 1996, *J. Geophys. Res.* **101**, 24343, doi:10.1029/96JA02129.
Crooker, N. U., Gosling, J. T., and Kahler, S. W.: 1998, *J. Geophys. Res.* **103**, 301.
Crooker, N. U., Shodhan, S., Gosling, J. T., Simmerer, J., Lepping, R. P., and Steinberg, J. T., 2000, *Geophys. Res. Lett.* **27**, 3769.
Crooker, N. U., Forsyth, R., Rees, A., Gosling, J. T., and Kahler, S. W.: 2004, *J. Geophys. Res.* **109**, A06110, doi:10.1029/2004JA010426.
Crooker, N. U., Kahler, S. W., Larson, D. E., and Lin, R. P.: 2004, *J. Geophys. Res.* **109**, A03108, doi:10.1029/2003JA010278.
Crooker, N. U., Huang, C.-L., Lamassa, S. M., Larson, D. E., Kahler, S. W., and Spence, H. E.: 2004, *J. Geophys. Res.* **109**, A03107, doi:10.1029/2003JA010170.
Crooker, N. U.: 2005, *Proc. Solar Wind 11*, *ESA-SP*, **592**, 289.
Crooker, N. U., and Horbury, T. S.: 2006, *Space Sci. Rev.*, this volume, doi: 10.1007/s11214-006-9014-0.
Farrugia, C. J., *et al.*: 2001, *Adv. Space Res.* **28**(5), 759.
Fenimore, E. E.: 1980, *Astrophys. J.* **235**, 245.
Feuerstein, W. M., Larson, D. E., Luhmann, J. G., Lin, R. P., Kahler, S. W., and Crooker, N. U.: 2004, *Geophys. Res. Lett.*, **31**, doi: 10.1029/2004GL020529.
Forbes, T. G., Linker, J. A., Chen, J., Cid, C., Kóta, J., and Lee, M. A., 2006, *Space Sci. Rev.*, this volume, doi: 10.1007/s11214-006-9019-8.
Forsyth, R. J., Rees, A., Reisenfeld, D. B., Lepri, S. T., and Zurbuchen, T. H.: 2003, in: M. Velli, R. Bruno and F. Malara (eds.), *Solar Wind Ten*, AIP Conf. Proc. **679**, Mellville, N.Y., p. 715.
Forsyth, R. J., Bothmer, V., Cid, C., Crooker, N. U., Horbury, T. S., Kecskemety, K., 2006, *Space Sci. Rev.*, this volume, doi: 10.1007/s11214-006-9022-0.
Galvin, A. B.: 1997, *Geophysical Monograph 99*. N. Crooker, J. A. Joselyn and J. Feymman (eds.), p. 253.
Geiss, J., Hirt, P., and Leutwyler, H.: 1970, *Sol. Phys.* **12**, 458.

Geiss, J., Bühler, F., Cerutti, H., Eberhard, P., and Filieux, C.: 1970b, *Sci. Rep. NASA SP* **315**, 14-1.
Geiss, J.: 1982, *Space Sci. Rev.* **33**, 201.
Geiss, J., Gloeckler, G., and von Steiger, R. : 1995, *Space Sci. Rev.* **72**, 49.
Gloeckler, G., Fisk, L. A., Hefti, S., Schwadron, N. A., Zurbuchen, T. H., and Ipavich, F. M. 1999, *Geophys. Res. Lett.* **26**(2), 157.
Gold, T.: 1959, *J. Geophys. Res.* **64**, 1665.
Goldstein, H.: 1983, in: M. Neugebauer (ed.), *Solar Wind Five*, NASA Conf. Publ. **22**, 731.
Gopalswamy, N., Lara, A., Yashiro, S., Nunes, S., and Howard, R. A.: 2003, in: A. Wilson (ed.), *Proc. ISCS 2003 Symp., Solar Variability as an Input to the Earth's Environment*, **ESA SP-535**, 419.
Gosling, J. T.: 1990, in: C. T. Russell, E. R. Priest and L. C. Lee (eds.), *Physics of Magnetic Flux Ropes*, American Geophysical Union, Geophysical Monograph **58**, 343.
Gosling J. T. and McComas, D. J.: 1987, *Geophys. Res. Lett.* **14**, 355.
Gosling, J. T., and Forsyth, R. J.: 2001, *Space Sci. Rev.* **97**, 87.
Gosling, J. T., and Skoug, R. M.: 2002, *J. Geophys. Res.* **107**(A10), 1327, doi::10.1029/2002JA009434.
Gosling, J. T., Hundhausen, A. J., and Bame, S. J.: 1976, *J. Geophys. Res.* **81**, 2111.
Gosling, J. T., Asbridge, J. R., Bame, S. J., Feldman, W. C., and Zwickl, R. D.: 1980, *J. Geophys. Res.* **85**, 3431.
Gosling, J. T., Baker, D. N., Bame, S. J., Feldman, W. C., Zwickl, R. D., and Smith, E. J.: 1987, *J. Geophys. Res.* **92**, 8519.
Gosling, J. T., Thomsen, M. F., Bame, S. J., and Zwickl, R. D.: 1987, *J. Geophys. Res.* **92**, 12399.
Gosling, J. T., Bame, S. J., McComas, D. J., and Phillips, J. L.: 1990, *Geophys. Res. Lett.* **17**, 901.
Gosling, J. T., Bame, S. J., Feldman, W. C., McComas, D. J., Phillips, J. L., and Goldstein, B. E.: 1993, *Geophys. Res. Lett.* **20**, 2335.
Gosling, J. T., Bame, S. J., McComas, D. J., Phillips, J. L., Scime, E. E., and Pizzo, V. J., 1994, *Geophys. Res. Lett.* **21**, 237.
Gosling, J. T., Birn, J., and Hesse, M.: 1995, *Geophys. Res. Lett.* **22**, 869.
Gosling, J. T., McComas, D. J., Phillips, J. L., Pizzo, V. J., and Goldstein, B. E., 1995, *Geophys. Res. Lett.* **22**, 1753.
Gosling, J. T., Skoug, R. M., and Feldman, W. C.: 2001, *Geophys. Res. Lett.* **28**, 4155.
Gosling, J. T., Skoug, R. M., McComas, D. J., and Smith, C. W.: 2005, *J. Geophys. Res.* **110**, A01107, doi:10.1029/2004JA010809.
Henke, T., Woch, J., Schwenn, R., Mall, U., Gloeckler, G., and von Steiger, *et al.*, 2001, *J. Geophys. Res.* **106**, 10597.
Hidalgo, M. A., Cid, C., Vinas, A. F., and Sequeiros, J.: 2002, *J. Geophys. Res.* **106**, DOI:10.1029/2001JA900100.
Hirshberg, J., Alksne, A., Colburn, D. S., Bame, S. J., and Hundhausen, A. J.: 1970, *J. Geophys. Res.* **75**, 1.
Hirshberg, J, Bame, S. J., and Robbins, D. E.: 1972, *Solar Phys.* **23**, 467.
Ho, G. C., Hamilton, D. C., Gloeckler, G., and Bochsler, P.: 2000, *Geophys. Res. Lett.* **27**, 309.
Hudson, H. S., Bougeret, J.-L., and Burkepile, J.: 2006, *Space Sci. Rev.*, this volume, doi: 10.1007/s11214-006-9009-x.
Hundhausen, A. J., Gilbert, H. E., and Bame, S. J.: 1968, *J. Geophys. Res.* **73**, 5485.
Huttunen, K. E. J., Schwenn, R., Bothmer, V., and Koskinen, H. E. J.: 2005, *Annales Geophysicae* **23**, 1.
Ipavich, F. M., Galvin, A. B., Gloeckler, G., Hovestadt, D., Bame, S. J. and Klecker, B., *et al.*, 1986, *J. Geophys. Res.* **91**, 4133.
Janoo, L. and Farrugia, C. J.: 1998, *J. Geophys. Res.* **103**, 17249.
Jian, L., Russell, C. T., Gosling, J. T., and Luhmann, J. G.: 2005, *American Geophysical Union*, Spring Meeting 2005, abstract #SH53A-11.
Jones, G. H., Balogh, A., and Forsyth, R. J.: 1998, *Geophys. Res. Lett.* **25**, 3109.

Jones G. H., Rees, A., Balogh, A., and Forsyth, R. J.: 2002, *Geophys. Res. Lett.* **29**(11), 10.1029/2001GL014110.
Jurac, S., and Richardson, J. D.: 2001, *J. Geophys. Res.* **106**, 29195.
Kahler, S.: 1977, *Astrophys. J.* **214**, 891.
Kahler, S. W. and Reames, D. V.: 1991, *J. Geophys. Res.* **96**, 9419.
Kahler, S. W., Crooker, N. U. and Gosling, J. T.: 1999, *J. Geophys. Res.* **104**, 9911.
Kasper, J. C.: 2003, 'Solar wind plasma : kinetic properties and micro-instabilities', Thesis (Ph. D.), Massachusetts Institute of Technology, Dept. of Physics, February 2003.
Klecker, B., Kunow, H., Cane, H. V., Dalla, S., Heber, B. and Kecskemety, K., *et al.*, 2006, *Space Sci. Rev.*, this volume, doi: 10.1007/s11214-006-9018-9.
Klein, L. W., and Burlaga, L. F.: 1982, *J. Geophys. Res.* **87**, 613.
Laming, J. M., and Feldman, U.: 2001, *Astrophys. J.* **546**, 552.
Lario, D., Hu, Q., Ho, G. C., Decker, R. B., Roelof, E. C., and Smith, C. W.: 2006, *Proc. Conf. Solar Wind 11, Whistler, Canada*, **ESA-SP-592**, 81.
Lario, D., Ho, G. C., Decker, R. B., Roelof, E. C., Desai, M. I., and Smith, C. W.: 2003, in: M. Velli, R. Bruno and F. Malara (eds.), *Proc. Conf. Solar Wind 10, Pisa, Italy*, **AIP-679**, American Institute of Physics, Melville, New York, p. 640.
Larson, D. E. *et al.*: 1997, *Geophys. Res. Lett.* **24**, 1911.
Lepping, R. P., Jones, J. A. and Burlaga, J. F.: 1990, *J. Geophys. Res.* **95**, 11957.
Lepping, R. P., *et al.*: 1997, *J. Geophys. Res.* **102**, 14049.
Lepping, R. P., Berdichevsky, D. B., Burlaga, L. F., Lazarus, A. J., Kasper, J., Desch, M. D., *et al.*: 2001, *Solar Physics* **204**(1–2), 285.
Lepri, S. T., Zurbuchen, T. H., Fisk, L. A., Richardson, I. G., Cane, H. V., Gloeckler, and G.: 2001, *J. Geophys. Res.* **106**(A12), 29231.
Lepri, S. T., and Zurbuchen, T. H.: 2004, *J. Geophys. Res.* **109**(A1), A01112.
Lindsay, G. M., Luhmann, J. G., Russell, C. T., and Gazis, P. R.: 1994, *J. Geophys. Res.* **99**, 11.
Lopez, R. E.: 1987, *J. Geophys. Res.* **92**, 11189
Low, B. C.: 1997, in: N. Crooker, J. A. Joselyn and J. Feynman (eds.), *Coronal Mass Ejections, Geophysical Monograph 99*, p. 39.
Low, B. C., and Zhang, M.: 2002, *Astrophys. J.* **564**, L53.
Manchester, W. B. and Zurbuchen, T. H.: 2006, *J. Geophys. Res.* **111**, A05101, doi:10.1029/2005JA011461.
Marsden, R. G., Sanderson, T. R., and Wenzel, K.-P.: 1985, *Proc. 19th Int. Cosmic Ray Conf.* **4**, 322.
Marsden, R. G., Sanderson, T. R., Tranquille, C., Wenzel, K.-P., and Smith, E. J.: 1987, *J. Geophys. Res.* **92**, 11009.
Martin, S. F., Bilimoria, R., and Tracadas, P. W.: 1994, *Solar Surface Magnetism*, Springer-Verlag, p. 303.
Marubashi, K.: 1986, *Adv. Space Res.* **6**, 335.
Marubashi, K.: 1997, in: N. Crooker, J. A. Joselyn and J. Feynman (eds.), *Coronal Mass Ejection, American Geophysical Union Geophys. Monogr.* Vol. 99, p. 147.
Mazur, J. E., Mason, G. M., Dwyer, J. R., and von Rosenvinge, T. T. 1998, *Geophys. Res. Lett.* **25**, 2521.
McComas, D. J., Gosling, J. T., Bame, S. J., Smith, E. J., and Cane, H. V.: 1989, *J. Geophys. Res.* **94**, 1465.
McComas, D. J., *et al.*: 1989, *J. Geophys. Res.* **94**, 6907.
Mitchell, D. G., Roelof, E. C., and Bame, S. J.: 1983, *J. Geophys. Res.* **88**, 9059.
Moldwin, M. B., Phillips, J. L., Gosling, J. T., Scime, E. E., McComas, D. J., and Bame, S. J., 1995, *J. Geophys. Res.* **100**, 19903.
Moldwin, M. B., Ford, S., Lepping, R., Slavin, J., and Szabo, A.: 2000, *Geophys. Res. Lett.* **27**, 57.
Montgomery, M. D., Asbridge, J. R., Bame, S. J., and Feldman, W. C.: 1974, *J. Geophys. Res.* **79**, 3103.
Morrison, P.: 1954, *Phys. Rev.* **95**, 646.

Mulligan, T., and Russell, C. T.: 2001, *J. Geophys. Res.* **106**, 10581.
Mulligan, T., Russell, C. T., and Luhmann, J. G.: 1998, *Geophys. Res. Lett.* **25**, 2959.
Nakagawa T., Nishida, A., and Saito, T.: 1989, J. Geophys. Res. **94**, 11761.
Neugebauer, M.: 1981, *Fundam. Cosmic Phys.* **7**, 131.
Neugebauer, M.: 1992, E., Marsch and R., Schwenn, (eds.), *Proceedings of Solar Wind 7*, p. 69.
Neugebauer, M., and Goldstein, R.: 1997, in N. Crooker, J. A. Joselyn and J. Feynman (eds.), *Coronal Mass Ejections*, AGU, Washington D.C., p. 245.
Neugebauer, M., and Liewer, P. C.: 2003, *J. Geophys. Res.* **108**(A1), 1013, doi:10.1029/2002JA009326.
Neugebauer M., Clay, D. R. and Gosling, J. T.: 1993, *J. Geophys. Res.* **98**(A6), 9383.
Neugebauer, M., Goldstein, R., and Goldstein, B. E.: 1997, *J. Geophys. Res.* **102**, 19743.
Neugebauer, M., *et al.*: 2003, *Space Science Reviews* **105**, 661.
Neukomm, R. O.: 1998, *Composition of Coronal Mass Ejections Derived with SWICS/Ulysses*. Ph. D. thesis, Universität Bern.
Osherovich, V. A., Fainberg, J., and Stone, R. G.: 1999, *Geophys. Res. Lett.* **26**, 401.
Owens, M., and Cargill, P., 2004, *Ann. Geophys.* **22**, 4397.
Phillips, J. L., and Gosling, J. T.: 1990, *J. Geophys. Res.* **95**, 4217.
Pilipp, W. G., Miggenrieder, H., Mülhäuser, K.-H., Rosenbauer, H., Schwenn, R., and Neubauer, F. M.: 1987, *J. Geophys. Res.* **92**, 1103.
Pizzo, V. J.: 1991, *J. Geophys. Res.* **96**, 5405.
Popecki, M., Desai, M., Skoug, R. M., Smith, C. W., Moebius, E., and Galvin, A. B., 2001, *Proc. 27th International Cosmic Ray Conference*, Hamburg, p. 3153.
Rao, U. R., McCracken, K. G., and Bukata, R. P.: 1967, *J. Geophys. Res.* **72**, 4325.
Reinard, A. A.: 2005, *Astrophys. J.* **620**, 501.
Reisenfeld, D. B., Steinberg, J. T., Barraclough, B. L., Dors, E. E., Wiens, R. C., and Neugebauer, M., 2003, *AIP Conf. Proc. 679: Solar Wind Ten* **679**, 632.
Richardson, I. G.: 1997, in: N. U. Crooker, J.-A. Joselyn and J. Feynman (eds.), *Coronal Mass Ejections*, Vol. 99, AGU., Washington D.C., p. 189
Richardson, I. G., and Cane, H. V.: 1993, *J. Geophys. Res.* **98**, 15295.
Richardson, I. G., and Cane, H. V.: 1995, *J. Geophys. Res.* **100**, 23397.
Richardson, I. G., and Cane, H. V.: 1996, *J. Geophys. Res.* **101**, 27521.
Richardson, I. G., and Cane, H. V.: 2004, *J. Geophys. Res.* **109**, A09104, doi:10.1029/2004JA010598.
Richardson, I. G., and Cane, H. V.: 2004, *Geophys. Res. Lett.* **31**, L18804, doi:10.1029/2004GL020958.
Richardson, I. G., Cane, H. V., and von Rosenvinge, T. T.: 1991, *J. Geophys. Res.* **96**, 7853.
Richardson, I. G., Cane, H. V., Lepri, S. T., Zurbuchen, T. H., and Gosling, J. T.: 2003, in: M. Velli, R. Bruno and F. Malara (eds.), *Solar Wind Ten*, AIP Conf. Proc. 679, Mellville, N.Y., p. 681.
Riley, P., and Crooker, N. U.: 2004, *Astrophys. J.*, in press.
Riley, P., *et al.*: 2002, *Astrophys. J.* **578**.
Riley, P., Linker, J. A., Mikic', Z., Odstrcil, D., Zurbuchen, T. H., Lario, D., Lepping, R. P.: 2003, *J. Geophys. Res.* **108**(A7), 1272, doi:10.1029/2002JA009760.
Riley, P., Linker, J. A., Lionello, R., Mikic, Z., Odstrcil, D., and Hidalgo, M. A., *et al.*, 2004, Accepted for publication in the *Journal of Atmospheric and Solar Terrestrial Physics*.
Rodríguez-Pacheco, J., Cid, C., Blanco, J. J., and Sequeiros, J.: 2003, *Sol. Phys.* **213**, 121.
Rodriguez, L., Woch, J., Krupp, N., Fänz, M., von Steiger, R., and Forsyth, R. J., *et al.*, 2004, *J. Geophys. Res.* **109**, A01108, doi:10.1029/2003JA010156.
Russell, C. T., Mellott, M. M., Smith, E. J., and King, J. H.: 1983, *J. Geophys. Res.* **88**, 4739.
Rust, D. M., and Kumar, A.: 1994, *Solar Phys.* **155**, 69.
Rust, D. M., Anderson, B. J., Andrews, M. D., Acuna, M. H., Russell, C. T., Schuck, P. W., *et al.*, 2005, *Astrophys. J.* **621**, 524.

Tripathi, D. K., Bothmer, V., and Cremades, H.: 2004, *Astron. & Astrophys.* **422**, 337.
Schwenn, R.: 1990, R., Schwenn, and E., Marsch, (eds.), *Physics of the Inner Heliosphere* I Springer-Verlag, Berlin, Heidelberg, p. 99.
Schwenn, R.: 1996, in: D. Winterhalter, J. T. Gosling, S. Habbal, W. S. Kurth and M. Neugebauer (eds.), *Solar Wind Eight*, Melville, New York, p. 426.
Schwenn, R., Rosenbauer, H., and Mühlhäuser, K.-H.: 1980, *Geophys. Res. Lett.* **7**, 201.
Sheeley, N. R. Jr., Howard, R. A., Koomen, M. J., Michles, D. J., Schwenn, R., and Mühlhäuser, K.-H.: 1985, *J. Geophys. Res.* **90**, 163.
Shodhan, S., *et al.*: 2000, *J. Geophys. Res.* **105**, 27261.
Siscoe, G.: 2006, *Space Sci. Rev.*, this volume.
Skoug, R. M., Bame, S. J., Feldman, W. C., Gosling, J. T., McComas, D. J., Steinberg, J. T., *et al.*: 1999, *Geophys. Res. Lett.* **26**(2), 161.
Smith, C. W., Ness, N. F., Burlaga, L. F., Skoug, R. M., McComas, D. J., Zurbuchen, T. H., *et al.*: 2001, *Sol. Phys.* **204**, 229.
Stansberry, J. A., Gosling, J. T., Thomsen, M. F., Bame, S. J., and Smith, E. J.: 1988, *J. Geophys. Res.* **93**, 1975.
St. Cyr, O. C., *et al.*: 2000, *J. Geophys. Res.* **105**, 18169.
Szabo, A., Smith, C. W., Tokar, R. L., and Skoug, R. M.: 1999, *Eos Transactions, American Geophysical Union* **80**(17) Supplement, S265.
Szabo, A., Lepping, R. P., Merka, J., Smith, C. W., and Skoug, R. M.: 2001, in: B. Battrick and H. Sawaya-Lacoste (eds.), *Solar Encounter, Proceedings of the First Solar Orbiter Workshop*, **ESA SP-493**, Noordwijk, ESA Publications Division, ISBN 92-9092-803-4, p. 383.
Vandas, M., and Romashets, E. P.: 2003, *Astron. Astrophys.* **398**, 801.
Vasquez, B. J., *et al.*: 2001, *J. Geophys. Res.* **106**, 29283.
von Steiger, R.: 1998, *Space Sci. Rev.* **85**, 407.
Wang, C., Richardson, J. D., Burlaga, L. F., and Ness, N. F.: 2003, *J. Geophys. Res.* **108**(A5), 1205, doi:10.1029/2002JA009809.
Wang, Y.-M., Sheeley, N. R., Jr., J. Walters, H., Brueckner, G. E., Howard, R. A., Michels, D. J., *et al.*: 1998, *Astrophys. J.* **498**, L165.
Wang, Y.-M., Sheeley, N. R., Jr., Socker, D. G., Howard, R. A., and Rich, N. B.: 2000, *J. Geophys. Res.* **105**, 25133.
Wang, Y. M., Wang, S., and Ye, P. Z.: 2002 *Sol. Phys.* **211**, 333.
Webb, D. F., Burkepile, J., Forbes, T. G., and Riley, P.: 2003, *J. Geophys. Res.* **108**(A12), 1440, 10.1029/2003JA009923,16 December 2003.
Webb, D. F., Cliver, E. W., Crooker, N. U., St. Cyr, O. C., and Thompson, B. J.: 2000, *J. Geophys. Res.* **105**, 7491.
Widing, K. G., and Feldman, U.: 2001, *Astrophys. J.* **555**, 426.
Wimmer-Schweingruber R. F.: 1994, 'Oxygen, Helium, and Hydrogen in the Solar Wind: SWICS/Ulysses Results', PhD thesis, University of Bern, Switzerland.
Wimmer-Schweingruber R. F., von Steiger, R., and Paerli, R.: 1997, *J. Geophys. Res.* **102**, 17407.
Wimmer-Schweingruber R. F., von Steiger, R., Geiss, J., Gloeckler, G., Ipavich, F. M., and Wilken, B.: 1998, *Space Sci. Rev.* **85**, 387.
Wimmer-Schweingruber R. F., Bochsler, P., Gloeckler, G., Ipavich, F. M., Geiss, J., Fisk, L. A., *et al.*: 1999a, *Geophys. Res. Lett.* **26**, 165.
Wimmer-Schweingruber R. F., Kern, O., and Hamilton, D. C.: 1999b, *Geophys. Res. Lett.* **26**, 3541.
Wimmer-Schweingruber R. F., von Steiger, R., and Paerli, R.: 1999c, *J. Geophys. Res.* **104**, 9933.
Winterhalter, D., Smith, E. J., Burton, M. E., Murphy, N., and McComas, D. J.: 1994, *J. Geophys. Res.* **99**, 6667.
Wu, C. C., Lepping, R. P., and Gopalswamy, N.: 2003, A., in: Wilson, (ed.), *Proc. ISCS 2003 Symp., Solar Variability as an Input to the Earth's Enviornment*, **ESA SP-535**, p. 429.

Wurz, P., Ipavich, F. M., Galvin, A. B., Bochsler, P., Aellig, M. R., and Kallenbach, R., *et al.*, 1998, *Geophys. Res. Lett.* **25**, 2557.

Wurz, P., Bochsler, P., and Lee, M. A.: 2000, *J. Geophys. Res.* **105**, 27239.

Wurz, P., Wimmer-Schweingruber, R. F., Issautier, K., Bochsler, P., Galvin, A. B., Paquette, J. A., and Ipavich, F. M.: 2001, *AIP conference proceedings* **598**, 145.

Zhang, G. and Burlaga, L. F.: 1988, *J. Geophys. Res.* **93**, 2511.

Zwickl, R. D., Asbridge, J. R., Bame, S. J., Feldman, W. C., and Gosling, J. T.: 1982, *J. Geophys. Res.* **87**, 7379.

Zwickl, R. D., Asbridge, J. R., Bame, S. J., Feldman, W. C., Gosling, J. T., and Smith, E. J.: 1983, in: M. Neugebauer (ed.), *Solar Wind Five; NASA Conference Proceedings 2280*, NASA, Washington, D.C., p. 711.

Zurbuchen, T., Fisk, L. A., Lepri, S. T., and von Steiger, R.: 2003, in: M. Velli, R. Bruno and F. Malara (eds.), *Solar Wind Ten*, AIP Conf. Proc. 679, Mellville, N.Y., p. 604.

Zurbuchen, T. H., Raines, J., Lynch, B., Lepri, S., Gloeckler, G., and Fisk, L.: 2005, 'In situ observation of filament plasma and their magnetic structure', *American Geophysical Union, Spring Meeting 2005*, abstract #SH54B-04.

Zurbuchen, T. H. and Richardson, I. G.: 2006, *Space Sci. Rev.*, this volume, doi: 10.1007/s11214-006-9010-4.

Zwickl, R. D., Doggett, K. A., Sahm, S., Barrett, W. P., Grubb, R. N., Detman, T. R., *et al.*: 1998, *Space Sci. Rev.* **86**, 633.